JCI insight

Increased lipogenesis and impaired β-oxidation predict type 2 diabetic kidney disease progression in American Indians

Farsad Afshinnia, … , Matthias Kretzler, Subramaniam Pennathur

JCI Insight. 2019. https://doi.org/10.1172/jci.insight.130317.

Clinical Medicine | In-Press Preview | Metabolism | Nephrology

Graphical abstract

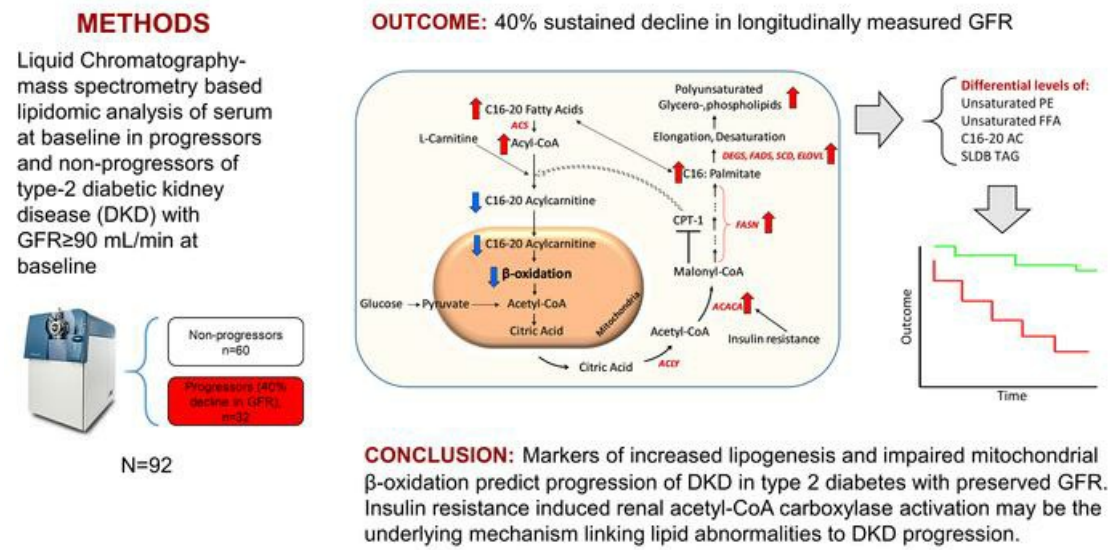

Increased lipogenesis and impaired β-oxidation predict type 2 diabetic kidney disease progression in American Indians

Authors:

Farsad Afshinnia[1], Viji Nair[1], Jiahe Lin[2], Thekkelnaycke M. Rajendiran[3,4], Tanu Soni[3], Jaeman Byun[1], Kumar Sharma[5], Patrice E. Fort[6], Thomas W. Gardner[6], Helen C. Looker[7], Robert G. Nelson[7], Frank C. Brosius[8], Eva L. Feldman[9], George Michailidis[10], Matthias Kretzler[1], Subramaniam Pennathur[1,3,11]

Affiliations:
[1]University of Michigan, Department of Internal Medicine-Nephrology, Ann Arbor, MI, USA
[2]University of Michigan, Department of Statistics, Ann Arbor, MI, USA
[3]University of Michigan, Michigan Regional Comprehensive Metabolomics Resource Core, Ann Arbor, MI, USA
[4]University of Michigan, Department of Pathology, Ann Arbor, MI, USA
[5]Department of Internal Medicine-Nephrology, University of Texas Health at San Antonio, San Antonio, TX, USA
[6]Department of Ophthalmology and visual sciences, University of Michigan, Ann Arbor, MI, USA
[7]Chronic Kidney Disease Section, National Institute of Diabetes and Digestive and Kidney Diseases, Phoenix, AZ, USA
[8]Department of Medicine, Division of Nephrology, University of Arizona, Tuscan, AZ, USA
[9]Department of Neurology, University of Michigan, Ann Arbor, MI, USA
[10]Department of Statistics and the Informatics Institute, University of Florida, Gainesville, FL, USA
[11]University of Michigan, Department of Molecular and Integrative Physiology, Ann Arbor, MI, USA

Address Correspondence to:
Subramaniam Pennathur, Division of Nephrology, 5309 Brehm Center, 1000 Wall Street, University of Michigan, Ann Arbor MI 48105 Email: spennath@umich.edu Phone (734) 936-5645 Fax (734) 232-8175

Running Title: Lipidomics and DKD

Word count: 11363
Tables: 3, **Figures:** 9, **Supplements:** 1

Support: Supported by the NIH grants R24DK082841, K08DK106523, R03DK121941, P30DK089503, P30DK081943, P30DK020572, the Program for Neurology Research and Discovery at Michigan Medicine (www.feldmanpnrd.org) and the Intramural Research Program of the National Institute of Diabetes and Digestive and Kidney Diseases.

Key words: Diabetes, Diabetic kidney disease, Lipidomics, Mass spectrometry, System biology

Role of funding agency: Financial support of the project

Abstract:

Background: In this study, we identified the lipidomic predictors of early type 2 diabetic kidney disease (DKD) progression, which are currently undefined.

Methods: This longitudinal study included 92 American Indians with type 2 diabetes. Serum lipids (406 from 18 classes) were quantified using mass spectrometry from baseline samples when iothalamate glomerular filtration rate (GFR) was ≥90 mL/min. Affymetrix GeneChip Array was used to measure renal transcript expression. DKD progression was defined as ≥40% decline in GFR during follow up.

Results: Participants had a mean age of 45±9 years and median urine albumin-creatinine ratio of 43 (interquartile range 11 to 144). The 32 progressors had significantly higher relative abundance of polyunsaturated triacylglycerols (TAG)s and a lower abundance of C16-20 acylcarnitines (AC)s ($p<0.001$). In a Cox regression model, the main effect terms of unsaturated free fatty acids and phosphatidylethanolamines and the interaction terms of C16-20 ACs and short, low-double-bond TAGs by categories of albuminuria independently predicted DKD progression. Renal expression of acetyl-CoA carboxylase encoding gene (*ACACA*) correlated with serum diacylglycerols in the glomerular compartment ($r=0.36$, $p=0.006$), and with low-double-bond TAGs in the tubulointerstitial compartment ($r=0.52$, $p<0.001$).

Conclusion: Collectively, the findings reveal a previously unrecognized link between lipid markers of impaired mitochondrial β-oxidation and enhanced lipogenesis and DKD progression, in individuals with preserved GFR. Renal acetyl-CoA carboxylase activation accompanies these lipidomic changes and suggests that it may be the underlying mechanism linking lipid abnormalities to DKD progression.

Funding: R24DK082841, K08DK106523, R03DK121941, P30DK089503, P30DK081943, P30DK020572

Trial Registration: ClinicalTrials.gov, NCT00340678

Introduction:

Diabetes is the leading cause of end-stage kidney disease in the United States and many other parts of the world (1). According to the 2018 United States Renal Data System report, the prevalence of end-stage kidney disease from diabetes continues to increase (2) and is expected to increase by 44% by 2030 (3). Efforts aimed at risk modification and halting diabetic kidney disease (DKD) progression are focused on the early stages of DKD, when treatment to slow disease development may be most successful. Clinical care of DKD patients presently relies on traditional biomarkers such as estimated glomerular filtration rate (eGFR) and urine albumin-creatinine ratio (ACR), which have limited precision and prognostic value early in the disease. Accordingly, there is a need for biomarkers that predict DKD progression early in its course for proper risk stratification and for rational targeted intervention.

Lipid studies in human clinical research are often limited to measuring a traditional panel of lipids, including total cholesterol, lipoproteins, and total triacylglycerols (TAG)s (4-8)). However, lipids are the most abundant and diverse class of molecules in the circulation with numerous physiological and metabolic functions (9, 10). Mass spectrometry (MS) based technological advances for identifying and quantifying lipids in biological samples have revealed the diversity of lipids, and also uncovered their clinical relevance in a number of diseases (9-17). In a cross-sectional study of 214 patients from the Clinical Phenotyping and Resource Biobank Core (CPROBE) cohort with chronic kidney disease (CKD), we found progressive differences in the human plasma lipidome from CKD stage 2 to stage 5 (18). In particular, we demonstrated an increase in the abundance of C16-C20 saturated free fatty acids (FFA) and polyunsaturated longer chain complex lipids in the later stages of CKD. In more advanced CKD, this lipid phenotype was associated with a lower long (C16-20)-to-intermediate chain (C6-C14)

acylcarnitine (AC) ratio, a marker of impaired β-oxidation of long chain (C16-C20) fatty acids. This leads to an increased abundance of C16-C20 carbon FFAs, rather than their acylation with carnitine to generate ACs and longer polyunsaturated complex lipids (18). In the lipidomic analysis of the Chronic Renal Insufficiency Cohort (CRIC), we found a higher abundance of phosphatidylethanolamines (PE)s in progressors compared to non-progressors (19). While there have been several efforts to identify progressive renal decline in diabetic patients with impaired renal function (19-24), less is known about the mechanisms, determinants and markers of early decline in patients with preserved renal function. Early decline was studied recently by the Joslin group and markers of tubular damage were identified as predictors of progression (23, 25). The central hypothesis of our present study was that the differential lipid alterations observed at more advanced DKD stages are a continuum of a process that starts prior to the onset of clinical DKD. Additionally, lipid alterations identified earlier may serve as markers of early DKD progression when traditional biomarkers such as eGFR and urine ACR are still normal. DKD has been characterized extensively over many years in American Indians from the Gila River Indian Community (26-31). In the present study, we examined the lipidomic predictors of DKD progression in this cohort. We hypothesized, based on our earlier observations (18, 19) that a subset of ACs, TAGs, FFA, and PEs would predict DKD progression at an early stage in patients with type 2 diabetes with preserved GFR (>90 mL/min) and normal urinary albumin excretion (ACR<30 mg/g). The presence of extensive clinical phenotyping and longitudinal follow-up, and the availability of matched serum and kidney biopsy specimens at a time when renal function is well-preserved, makes this cohort ideal for performing systems integration of lipidomic and renal lipid gene expression profiling. Our studies reveal previously unrecognized novel lipidomic signature of early DKD progression.

Results:

Patient characteristics: American Indians from the Gila River Indian Community participated in a longitudinal study of diabetes and its complications. 169 of the study participants were recruited between 1996 and 2001 for a randomized, double-blind, placebo-controlled, clinical trial to assess the efficacy of the angiotensin receptor blocker losartan on onset and progression of diabetic nephropathy in type 2 diabetes (ClinicalTrials.gov, number NCT00340678). Iothalamate based GFR was measured annually (32, 33). Of 169 participants in the clinical trial, 111 underwent a protocol kidney biopsy at the end of 6 years of treatment. We selected 92 participants who underwent a kidney biopsy and had both a GFR ≥90 mL/min and serum samples available that had been collected during the GFR measurement taken closest to the kidney biopsy. This examination was considered the baseline (Figure 1). The primary outcome was defined as a sustained decline in GFR by 40% in follow up examinations, an outcome which is accepted as a surrogate marker of CKD progression (34). Time to event was defined as the interval between the date of baseline GFR measurement and the date of the primary outcome. A GFR<90, <60, and <30 mL/min were defined as secondary outcomes. The 92 participants, including 67 women and 25 men, were followed for a maximum of 13.6 years (median 9.6 years and interquartile range 7.3 to 11.0 years). Their mean age was 45±9 years, and body mass index (BMI) was 36.1±8.3 kg/m^2 in the female participants and 34.2±7.9 kg/m^2 in the male participants (p=0.33). Thirty-two of the participants reached the primary renal outcome of 40% decline in measured GFR during follow up.

Baseline characteristics: The baseline characteristics of progressors and non-progressors are shown in Table 1. Most characteristics were similar in the two groups, except for statistically

higher mean diastolic blood pressure, fasting plasma glucose (FPG), HbA1c, GFR, and urine ACR in the progressors. Baseline and last measured GFRs for both groups are shown in Figure 2.

Baseline lipidomic profile of progressors and non-progressors: We measured 406 lipids from 18 classes including TAGs, diacylglycerols (DAG)s, monoacylglycerols (MAG)s, phosphatidylcholines (PC)s, PEs, plasmenyl-PCs (pPC)s, plasmenyl-PEs (pPE)s, lyso-PCs (LPC)s, lyso-PEs (LPE)s, FFAs, cholesteryl-esters (CE)s, cardiolipins, phosphatidic acids (PA)s, phosphatidylinositols (PI)s, phosphatidylglycerol (PG)s, phosphatidylserine (PS)s, sphingomyelins (SM)s, and ceramide-phosphates in positive and negative ionization modes (Supplement Table 1). After combining the different adducts of the same feature and eliminating the classes consisting of 2 or fewer lipid molecules (PA, PG, PS, pPC, ceramide phosphate, and MAG), 236 unique lipids including 16 FFAs (6.8%), 76 glycerolipids (32.2%), 83 phospholipids (35.1%), 12 CEs (5.1%), 20 SM (8.5%), and 29 ACs (12.3%) were included in the analysis.

In progressors (≥40% decline in GFR), there was a higher relative abundance of longer TAGs with more double bonds ($p<0.0001$) (Figure 3A). Conversely, in non-progressors there was a lower relative abundance of longer TAGs with more double bonds at baseline ($p=0.022$) (Figure 3A). The alterations in lipid abundance by carbon number or saturation status were independent of baseline GFR, ACR, weight, FPG, and HbA1c. Similar alterations in the relative abundance of TAGs were observed when all participants were divided based on whether they reached a sustained GFR<90 mL/min, <60 mL/min, or <30 mL/min with stronger trends with increased CKD severity ($p<0.0001$) (Figure 3B). There were no significant alterations between progressors and non-progressors in the levels of other complex lipids by differences in the number of carbons or double bonds.

Baseline AC profiles in progressors and non-progressors: For the primary outcome of ≥40% GFR decline (Figure 3C), there was a significantly lower abundance of serum ACs with a longer chain length (C16-20) in progressors ($p<0.001$). Conversely, the non-progressors exhibited a higher abundance of serum ACs with longer chain length ($p=0.026$). These changes were inverse to the alterations observed in TAGs in progressors and non-progressors. Similar changes in the abundance of longer chain length ACs (C16-20) were observed when all participants were divided based on whether they reached a sustained GFR<90 mL/min (Figure 3D, left panel), <60 mL/min (Figure 3D, middle panel), or <30 mL/min (Figure 3D, right panel). Overall, the abundance of C16-C20 ACs was significantly lower in participants who reached the GFR threshold compared to those who did not ($p\leq0.015$), suggesting impaired β-oxidation.

Baseline long-chain-to-intermediate-chain AC ratio correlation with chain length and saturation of other complex lipids: The data in figure 3A-D suggest that the abundance of longer chain ACs correlates directly with shorter TAGs and inversely with longer TAGs. We also examined the correlation of the long-to-intermediate chain ACs with different principal components (Supplement Table 2) characterized by their length and saturation status. We found a significant direct correlation between long-to-intermediate chain AC ratio and the short complex lipids with fewer double bonds in the TAG, pPE, PE, and DAG lipid classes (Figure 4). We also observed a significant inverse correlation between long-to-intermediate chain AC and the longer chain complex lipids with more double bonds in the CE classes (Figure 4).

Alteration of ACs by categories of urinary ACR: The abundance of ACs in progressors and non-progressors by change in number of carbons and double bonds was also compared when stratified by the baseline ACR category (Figure 5). The heat map suggests a trend toward lower levels of long chain ACs (C16-20) from non-progressors with ACR<30 mg/g to progressors with

ACR>300 mg/g. Within each ACR category, the change in AC abundance by increased carbon number reached statistical significance and increased in non-progressors with ACR 30-299 mg/g ($p=0.006$), and decreased in progressors with ACR>300 mg/g ($p<0.0001$). Overall, the mean level of C16-20 ACs in progressors with ACR>300 mg/g was significantly lower than in any other subgroup ($p\leq0.004$), except non-progressors with ACR>300 mg/g where the difference did not reach statistical significance.

Risk prediction of DKD progression from lipid changes: We used the lipid principal components (Supplement Table 2) to construct Cox regression models for risk prediction of DKD progression. We applied different models with varying levels of adjustment. First, we built the base model, which included the study principal components without adjusting for the clinical variables (Table 2, Model 1: ACR+GFR). In this model, each 1 standard deviation (SD) increase in unsaturated PEs was associated with 1.78-fold higher risk of progression (95% confidence interval [CI]: 1.24 to 2.57, $p=0.002$), and each 1 SD increase in unsaturated FFAs was associated with 0.66-fold lower risk of progression (95% CI: 0.46 to 0.95, $p=0.026$) independent of other lipid factors. In the next step, we identified the principal components with a significant interaction term by ACR category and then added them to the base model (Table 2, Model 2: Lipids). By doing so, we observed strengthening of the significance of unsaturated PEs and unsaturated FFAs. However, we also noted that each 1 SD increase in C16-20 ACs in participants with ACR<30 mg/g, compared to ACR≥300 mg/g, was associated with a 3.36-fold higher risk of DKD progression (95% CI: 1.00 to 11.28, $p=0.05$). Similarly, each 1 SD increase in short low double bond TAGs was associated with significantly lower risk of progression in participants with ACR<30 or ACR 30-299 mg/g compared to ACR≥300 mg/g (Table 2, Model 2: Lipids). Further adjusting using baseline GFR, ACR, FPG, and HbA1c did not alter the results

and similar estimations were obtained in the fully adjusted model (Table 2, Model 3; ACR+GFR+Lipids).

Next, we compared the probabilistic risk scores of progressors and non-progressors obtained from these 3 models. Model 3 (ACR+GFR+Lipids) showed the largest difference between the risk score of progressors and non-progressors, on average, compared with the other two models (Figure 6A). When percentage with progression was compared by the risk-score quartiles, the first quartile of the full model was more likely to consist of non-progressors and its fourth quartile was more likely to consist of progressors compared to the other two models (Table 3).

Differential network analysis: To understand changes in the potential interactions between lipids, we performed differential network analysis using sparse correlations networks in the progressor and non-progressor subgroups. The differential network analysis revealed a significant loss of inter and intra-class correlation of lipids in progressors compared to non-progressors. This was observed most frequently in the TAG, PE, and AC subclasses and, to a lesser extent, in other subclasses (Figure 7). Overall, out of 55,460 possible permutations of bivariate correlations in 236 lipids, non-progressors had 1028 significant edges while progressors had 547 ($p<0.0001$). Among classes with at least five significant correlations with other lipids, there were 519 significant edges in non-progressors and 287 edges in progressors, a 50% decline ($p<0.0001$).

Systems integration of renal transcriptomics and serum lipidomics: Because a protocol kidney biopsy taken near the time of baseline serum collection was available, we had the unique opportunity to perform an integrative transcriptomic analysis using dissected glomerular and tubulointerstitial kidney tissue and serum lipids. The transcriptomic-lipidomic analysis in the glomerular compartment revealed significant correlations between lipid factors, including FAs,

glycerolipids, and ACs with the genes regulating their synthesis and metabolism (Supplement Table 4). Specifically, a higher abundance of longer polyunsaturated DAGs was associated with higher gene expression of the acetyl-CoA carboxylase (*ACACA*; p=0.0062, FDR=0.060). Conversely, the abundance of long chain ACs was inversely correlated with expression of fatty acid metabolism encoding genes ($p \leq 0.0052$, $FDR \leq 0.052$). In the tubulointerstitial compartment, there were significant correlations between fatty acids, glycerolipids, phospholipids, and ACs and the expression of genes involved in the synthesis and metabolism of fatty acids, phospholipids, glycerolipids, and sterol lipids. There were a larger number of significant correlations between the genes responsible for *de novo* synthesis, desaturation, elongation, and β-oxidation of various serum fatty acids, glycerolipids, and long chain ACs (Supplement Table 5). Specifically, a higher abundance of intermediate-chain low-double-bond TAGs was associated with a higher *ACACA* expression (p=0.0042, FDR=0.009). Additionally, in the tubulointerstitial compartment, we noticed a significant direct correlation between fatty acid abundance in serum and the expression of genes responsible for *de novo* fatty acid biosynthesis (*ACSL5* and *LYPLA3* or *PLA2G15*) and their β-oxidation (*ACAD10*). We also observed a direct correlation between short-low-double bond DAGs and unsaturated FFAs and genes responsible for elongation (*ELOVL1* and *ELOVL5*) and desaturation (*DEGS1*). There were inverse correlations between high-double-bond TAGs and saturated FFA and genes coding elongation (*ELOVL1* and *ELOVL4*) and between short-low-double-bond DAGs and TAGs, unsaturated FFA, and long-chain AC and genes regulating β-oxidation (Supplement Table 5). Ingenuity Pathway Analysis based on the top lipid-transcripts revealed enrichment of G-Protein coupled signaling pathways as regulators of *de novo* lipogenesis in both glomerular (Figure 8A) and tubulointerstitial compartments (Figure 8B). The genes involved in lipid metabolism downstream of the nuclear

hormone-activated receptors peroxisome proliferator–activated receptor γ (*PPARG*) and peroxisome proliferator–activated receptor A (*PPARA*) were expressed with a high degree of similarity in both glomerular (Figure 8C) and tubulointerstitial compartments (Figure 8D), suggesting similar lipogenic processes are activated in both compartments by these upstream regulators.

Discussion:

We identified novel, previously unrecognized lipid predictors of progressive DKD in diabetic American Indians with preserved kidney function, as indicted by GFR≥90 mL/min. Lipid factors representative of unsaturated FFA and PEs, short-low-double-bond TAGs, and long-chain ACs predicted DKD progression in these patients. A transcriptomic-lipidomic integrative analysis revealed significant correlation between serum FFAs and genes regulating *de novo* fatty acid synthesis in the glomerular compartment. Similarly, the integrative analysis showed a significant correlation between serum FFAs, glycerolipids, and ACs and genes regulating *de novo* fatty acid synthesis, desaturation, elongation, and β-oxidation. Importantly, the gene regulating acetyl-CoA carboxylase (*ACACA*) was directly associated with long polyunsaturated DAGs in the glomerular compartment, and with low-double-bond intermediate-length TAGs in the tubulointerstitial compartment. The differential networks identified in the present study reflect a differential interactome among various lipids by status of DKD progression.

The results of this study carry significant clinical implications. While tubular markers have been proposed as indicators of early renal function decline, there are no known lipid predictors of DKD progression at a stage when GFR is preserved and other patients' characteristics are non-informative. The proposed panel accurately predicts DKD onset and progression and, therefore, may have clinical applicability for risk stratification in patients with diabetes. Second, the lipid markers unravel novel mechanism underlying DKD progression: impaired mitochondrial β-oxidation and altered complex lipid remodeling. Importantly, the ability to perform integrative renal gene expression with serum lipids was uncovered ACC activation as a critical determinant. Consequently, ACC inhibition might be a therapeutic

strategy to prevent DKD or slow its progression. Not all patients with diabetes develop DKD, therefore, the possible contribution of ACC polymorphisms to renal outcomes needs to be investigated. Furthermore, in an earlier study of this cohort, progressors were shown to have a higher mesangial fractional volume, percentage of global glomerular sclerosis, non-podocyte cell number per glomerulus, glomerular basement membrane width, mean glomerular volume, and podocyte foot process width. However, they had lower glomerular filtration surface density, with fewer endothelial fenestrations after adjustment for baseline age, sex, duration of diabetes, HbA1c, GFR, and treatment assignment during the clinical trial (26). Although, such early histological alterations provided a readout of future decline in renal function, lipid alterations provide a noninvasive readout of similar long-term outcomes and demonstrate potential for early stage risk stratification in clinical practice.

There are a number of similarities in the results of this study and our previous lipidomic study in CRIC (19). However, a few differences between these two studies are worth noting. At baseline examination, participants of CRIC had CKD stage 3A or 3B, while in this study all were at stage 1 (GFR>90 mL/min). Only 50% of the CRIC participants had type 2 diabetes, whereas every participant in this study has type 2 diabetes. FFAs and ACs were not measured in CRIC nor were kidney biopsies routinely obtained as part of research data collection. Despite these differences, we noted a higher risk of DKD progression at higher levels of unsaturated PEs in American Indians with diabetes, which is aligned with enrichment of PE as a class and its higher abundance in CKD progressors in the CRIC study (19). In a metabolomic investigation in participants of the African American Study of Kidney Disease and Hypertension (AASK) and the Modification of Diet in Renal Disease (MDRD), a significant enrichment of PEs was noted among the top metabolites associated with proteinuria in CKD patients (35). Aligned with these

observations, a diabetic mouse model showed accumulation of the Amadori-PEs species in tubular cells (36). The mechanistic link between PE and DKD progression has yet to be identified. However, PEs have diverse cellular functions including oxidative phosphorylation, mitochondrial biogenesis, and autophagy. PEs are phosphatidylcholines precursors, substrates for posttranslational modifications, influence membrane topology, and promote cell and organelle membrane fusion (37). Cell culture experiments also suggest that exposure to PE alters the plasma membrane bilayer with total loss of asymmetrical aminophospholipids, and promotes apoptosis (38) and autophagy (39).

Another finding in our study was a lower risk of DKD progression with higher unsaturated FFA abundance. This finding is aligned with earlier studies that illuminated salutary effects of longer unsaturated FFAs, such as oleate and eicosapentaenoic acid, on inflammation, endoplasmic reticulum stress, and eventually better podocyte and pancreatic cell survival compared with the effect of saturated FFA palmitate (40-43). In a cross-sectional analysis of the CPROBE study, we showed that at more advanced CKD stages, there was a significantly greater abundance of longer polyunsaturated TAGs and a lower abundance of C16-20 ACs (18). Patients at CKD stage 5 thus had the highest abundance of longer polyunsaturated TAGs and the lowest abundance of C16-20 ACs. Replication of this pattern was seen in this study in DKD progressors, but at a much earlier stage when GFR was still above 90 mL/min. In the CRIC study, although DAGs as a class were enriched in CKD progressors, TAGs were not significantly different (19), a finding inconsistent with CPROBE and the current study. A likely explanation is the narrow range of baseline GFRs in CRIC participants compared to the CPROBE study whose patients were at all stages, and the marked heterogeneity in CRIC enrollees compared to the homogeneity of American Indian cohort. TAGs differ in their renal toxicities by their acyl length

and number of double bonds, and in part by the characteristics of their acyl constituents, especially when they are non-esterified (prior to utilization in the construct of TAGs or after their lipolysis). Overall, the main renal toxicities are determined by saturated fatty acids such as palmitate, through mechanisms that involve activation of AMP-activated protein kinase (AMPK) and mammalian target of rapamycin complex-1 (mTOR1) signaling pathways. Furthermore, they can promote insulin resistance, mitochondrial superoxide generation, and endoplasmic reticulum stress. Other mechanisms of toxicity include impairment of the podocyte actin cytoskeleton, induction of autophagy, and eventual triggering of apoptosis and cell death (40, 42, 44-49). Within the tubulointerstitial compartment, palmitate upregulates the monocyte chemoattractant protein-1, leading to intracellular activation of DAG followed by protein kinase C(PKC), which further promotes renal tubular cell injury (43). Abundance of saturated fatty acids (specifically palmitate) upregulates the elongation and desaturation of shorter free fatty acids and their incorporation in the construct of TAGs. The longer polyunsaturated TAGs have a higher melting temperature with greater fluidity, and thus are less toxic than the non-esterified saturated fatty acids. Therefore, although they served as a surrogate marker of DKD progression, their higher abundance in progressors likely signifies upregulation of adaptive compensatory processes (elongation, desaturation) to convert more toxic lipids (saturated non-esterified fatty acids) into less toxic lipids (polyunsaturated long TAGs). The progressors were also characterized by lower abundance of shorter TAGs with fewer double bonds. This probably reflects a lower abundance of fatty acids with ≤14 carbons, which become the dominant mitochondrial substrates in progressors whose mitochondrial shuttling of fatty acids with ≥16 carbons is impaired due to carnitine palmitoyltransferase I (CPT-1)inhibition (50). This response leads to a relatively lower abundance, and thus lower likelihood of their incorporation into corresponding (short) TAGs.

Therefore, while the high abundance of longer polyunsaturated TAGs signifies upregulation of elongation and desaturation as compensatory mechanisms, the lower abundance of shorter and saturated TAGs reflects low abundance of the corresponding non-esterified fatty acids (≤14 C), which indicates impaired β-oxidation of fatty acids with ≥16 carbons. When stratified by levels of albuminuria, progressors with normal albumin excretion (ACR<30 mg/g) had significantly higher AC levels compared with progressors with overt proteinuria (ACR>300 mg/g), suggesting that β-oxidation may be upregulated as a compensatory mechanism in the early stages of DKD, but that β-oxidation becomes impaired over time with progression to overt proteinuria. These observations suggest that the lipid phenotype associated with advanced DKD may be a continuum that begins mechanistically at an early stage, allowing early discrimination of progressors from non-progressors and risk stratification during early kidney disease when no other prognostic tools are available.

The Ingenuity Pathway Analysis highlights the enrichment of the G-protein signaling pathways in both glomerular and tubulointerstitial compartments. G-Proteins promote transcriptional activation of metabolic genes by carbohydrate-response element-binding protein (ChREBP), and regulate downstream lipogenic genes, including acetyl-CoA carboxylase (*ACACA*), fatty acid synthetase, acyl CoA synthase and glycerol phosphate acyl transferase (https://www.ncbi.nlm.nih.gov/biosystems/1270101?Sel=geneid:2771#show=genes). In particular, the significant association of *ACACA* gene expression with DAGs in the glomerular and TAGs in the tubulointerstitial compartments supports the hypothesis that the observed differential serum lipids may be regulated, in part, by renal ACC. The direct correlation of shorter low double bond DAGs with elongase and desaturase imply that a higher abundance of such lipids may upregulate the renal cortical elongation and desaturation of fatty acids as a

compensatory mechanism that converts shorter and relatively more saturated, toxic lipids into longer, relatively more unsaturated, less toxic products. On the other hand, the direct correlation of saturated FFAs with *ACAD10,* a β-oxidation regulatory gene, suggests they may upregulate β-oxidation, at least in early-stage DKD, a process which may be reversed with DKD progression or by unsaturated FFAs, due to their inverse correlation with *ACAT2,* β-oxidation regulatory gene. Altogether, the differential lipid alterations associated with DKD progression suggest accelerated renal *de novo* lipogenesis and impaired β-oxidation (18).

Acceleration of *de novo* lipogenesis is a major contributor to dyslipidemia in insulin resistance states such as in type 2 diabetes (51). *De novo* lipogenesis of long-chain fatty acids is dependent on the activity of three cytosolic enzymes: ATP citrate lyase, ACC, and fatty acid synthetase (52). ACC is a key regulatory enzyme in lipogenesis and its activity is under hormonal regulation by insulin, glucagon, and epinephrine. During insulin-resistance, increased insulin promotes ACC activation via its protein-phosphatase mediated dephosphorylation (53). A recent expression Quantitative Trait Loci (eQTL) analysis of participants of Nephrotic Syndrome Study Network revealed a significant differential expression of G/C *ACACA* variant in both glomerular and tubulointerstitial compartments of the participants (54), suggesting possibility of *ACACA* polymorphism on ACC activity. ACC activation inhibits CPT-1, lowering cytosolic conversion of long-chain acyl-CoA to long-chain AC, decreased substrate for the carnitine shuttle, impaired β-oxidation of long-chain fatty acids, and increased cytosolic abundance of palmitate (52). Increased palmitate promotes elongation and desaturation, as evidenced by upregulation of stearoyl-CoA desaturase (*SCD*) 1 and 2 (Figure 9) (55). It also exerts its deleterious effects on podocytes and tubulointerstitial cells by upregulating AMPK and mTOR1 signaling, intracellular serial DAG and PKC activation, induction of mitochondrial superoxide

generation, endoplasmic reticulum stress, and, eventually, promotion of autophagy, apoptosis and cell death (40, 42, 43, 46-49).

Based on these data, we propose a model to account in part for these serum lipidomic changes that predict DKD progression (Figure 9). Upregulation of renal (and possibly liver) ACC in the diabetic milieu enhances *de novo* lipogenesis, which generates excess saturated fatty acids (*e.g.*, palmitate). Although kidney ACC expression is modified, the liver may also influence circulating levels of fatty acids and complex lipids. With elongation and desaturation, palmitate is converted to longer unsaturated fatty acids, which are incorporated into complex lipids (e.g., glycerolipids). In addition, ACC upregulation can inhibit CPT1, which impairs β-oxidation. Finally, elevated free fatty acids present in the diabetic state can exacerbate mitochondrial dysfunction, especially in the setting of impaired fatty acid oxidation. The net effect will be a pattern of complex lipid remodeling and diminished fatty acid β-oxidation, as observed in our studies.

This study has several strengths, including the longitudinal study design, rigorous quality control with good reproducibility metrics in a robust LC/MS lipidomic platform, and excellent phenotyping of a well-characterized cohort of type 2 diabetes patients. Yearly follow ups and iothalamate-based GFR measurements provided accurate evaluation of kidney outcomes. A kidney biopsy near the time of baseline serum collection permitted a novel integrative lipidomic-transcriptomic analysis. The availability of data and samples prior to the onset of clinical DKD provided the opportunity to identify early prognostic DKD markers.

This study also has limitations. Although existing knowledge of the *de novo* lipogenesis pathway, along with the results obtained from the transcriptomic-lipidomic integrative analysis, support the hypothesis that ACC activation may be responsible, in part, for the differential lipid

pattern, our results cannot distinguish whether the increased renal ACC expression is a cause or a consequence of the differential plasma lipid profile. In a recent study, we assessed individual lipid features present in plasma from control and diabetic *db/db* mice (56). Plasma lipid levels and DAG saturation status corresponded to kidney levels in diabetic mice compared to control, suggesting that plasma DAG metabolism may be reflected in the kidney. However, this relationship is not known in humans and technically not feasible to assess given the difficulty in obtaining adequate kidney biopsy specimen for lipidomic analysis. The study sample size is small, and replication of the study, including the risk prediction model, in larger cohorts and in other racial/ethnic groups is warranted. Like any other omic-type research, this study has a large number of variables due to the high-throughput data generated by the lipidomic platform. We applied a number of strategies to minimize the need for multiple testing including application of mixed-linear models to study alterations at the group level versus individual lipids, reducing the data to a smaller number of principal components for downstream analysis, partial correlation-based sparsing techniques for the study of the differential networking, and FDR correction for multiple testing in lipidomic-transcriptomic integrative analysis. Although we observed a significant interaction between categories of albuminuria in the risk prediction model, with advancing DKD, the differential lipid alterations were independent of proteinuria in our prior cross-sectional study (18). Routinely, frequency of follow up declines over time, and participants with worse kidney function tend to attend research examinations less often than participants with preserved kidney function, raising the possibility of differential censoring by outcome (29, 30). However, in this particular subset of participants, the duration and number of follow-up visits were almost equal in progressors and non-progressors, so the potential for ascertainment bias due to differences in follow up is low. The current study is also limited by its sample size to

investigate *ACACA* polymorphism despite evidence for *ACACA* polymorphism in other renal eQTL studies (54).

This study has important clinical implications and illustrated that a panel of lipid biomarkers may predict decline at early stage when kidney function is still preserved (GFR>90 mL/min). It provides a valuable opportunity for early stage risk stratification when there is a paucity of reliable biomarkers at early stage. The proposed underpinning mechanism suggests targeted interventions at early stage. Inhibition of kidney fibrosis by modulating fatty acid receptors (57) provides further encouraging evidence for the success of such interventions. We conclude that lipid alterations that typify advanced DKD are present before the onset of clinical DKD and are characterized by higher abundance of unsaturated PEs, longer polyunsaturated TAGs, but lower abundance of unsaturated FFAs and C16-20 ACs. In patients with GFR>90 mL/min, a panel of lipids consisting of unsaturated FFA and PEs, short-low-double-bond TAGs, and long-chain ACs predicts the onset and progression of DKD. The underlying mechanism may depend on impairment of fatty acid β-oxidation and renal ACC activation, thus providing a potential therapeutic target (Figure 9).

Methods:

Patients: Details of the study population and participant recruitment are published elsewhere (31).

Sample preparation and mass spectrometry: We applied previously published methods for sample preparation (18, 19, 58). In brief, we used the modified Bligh-Dyer method for lipid extraction. We retrieved 10 µL of serum and added water/methanol/dichloromethane at room temperature with 2:2:2 volume ratio, followed by spiking internal standards PC17:0/17:0, LPC 17:0, PG 17:0/17:0, PE 17:0/17:0, TAG 17:0/17:0/17:0, SM 18:1/17:0, MAG 17:0, DAG 16:0/18:1, CE 17:0, ceramide d 18:1/17:0, PA 17:0, PI 17:0/20:4, and PS 17:0/17:0. After collecting the organic layer, we dried the extracts under nitrogen and reconstituted them by adding 100 µL of acetonitrile/water/isopropyl alcohol (10:5:85) followed by 10 mM ammonium acetate (NH_4OAc). Then we subjected the extracts to liquid chromatography-mass spectrometry (LC/MS), utilizing ABSciex quadrupole time of flight (TOF)-5600 mass spectrometer equipped with a Turbo V^{TM} ion source (AB Sciex, Concord, Canada) and Shimadzu CTO-20A Nexera X2 UHPLC with water acquity UPLC HSS T3 1.8 µm column (Waters, Milford, MA). ACs were quantified by LC/MS using an Agilent 6410 Triple quadrupole tandem mass spectrometer (Agilent, Santa Clara, CA) with a targeted method described previously (59).

Quality Control: A pool of study samples was injected at the beginning and after every 20 MS runs in the lipidomic study and after every 15 MS runs in the AC study to assess the stability of the measures over time and to identify any batch effects (Supplement Figures 1 and 2).

Transcriptomic Analysis: We manually microdissected kidney biopsy specimens to isolate glomerular and tubulointerstitial tissue. Glomerular and tubular gene expression profiling was performed as described previously on Affymetrix Gene Chip Array Human Genome series

U133A and Plus 2.0 (Affymetrix, Inc., Santa Clara, CA) (60, 61). Cell files were processed, normalized (Robust Multi Array method) and batch corrected (COMBAT) on the R statistical platform. We used Human Entrez Gene custom CDF from Brainarray for annotations (http://brainarray.mbni.med.umich.edu/). Normalized and log2 transformed expression profiles were used in all the downstream analyses.

Statistical analysis: We applied mean ± SD or frequency (percentage) for description of normally distributed continuous and categorical variables, respectively. Median and interquartile range were used to describe non-normally distributed variables. To compare the baseline characteristics of progressors and non-progressors we used the t-test for normally distributed continuous variables, the Kolmogorov-Smirnov test for skewed continuous variables, and the chi-square test for categorical variables. We used the relative abundance of the peak intensities for the downstream analysis. To prepare the lipidomics data for downstream analysis, the batch normalized raw peak intensities were sum normalized by lipid members within each lipid sub-class, logit transformed, and z-score standardized (18). We used principal component analysis (PCA) to reduce the number of lipids of the TAG, DAG, PE, pPE, CE, FFA, and AC classes to subclasses to generate secondary variables representative of various chain lengths within these classes (Supplement Table 2). Long-chain AC (C16-C20)-to-intermediate-chain AC (C6-C14) ratio was applied as a marker of efficiency of β-oxidation (62). Multiple linear regression analysis was applied to explore the relationships between the long-chain-to-intermediate-chain AC ratio (predictor variable) with the resulting principal components (secondary variables) of complex lipids. We used generalized linear mixed models to test the intra-class alteration in lipid abundance (standardized, logit transformed, normalized lipid intensities used as the dependent

variable) by change in carbon number and number of double bonds (saturation status) as the predicting variables.

We applied a Cox proportional hazard model to identify the independent lipid predictors of DKD progression and to estimate the risk associated with their change. Violation to proportional hazard assumption was ruled out by confirming the random distribution of the scaled Schoenfeld residuals also known as partial residuals of the predicting variables over time. We adjusted the models by BMI, fasting plasma glucose (FPG), hemoglobin A1c (HbA1c), and ACR followed by elimination of non-significant covariates from the model. The probability of progression by various panels was estimated using the logit score of the corresponding predictors in each panel and their conversion to probabilistic risk scores (63). Risk score calculation was performed separately for the baseline ACR and GFR, the lipids proposed by Cox model, and the proposed lipids plus baseline ACR and GFR. The risk analysis was performed separately for the baseline model (Model 1: ACR+GFR), the model incorporated lipid components with a significant interaction term by ACR categories (Model 2: Lipids), and the model adjusted further by baseline GFR, ACR, FPG, and HbA1c (Model 3: ACR+GFR+Lipids).

Because baseline TAG levels were different between progressors and non-progressors, the glycerolipid factors and their upstream regulators (FFAs and ACs) were tested for their correlation with corresponding renal tissue transcripts. We used MetScape to map lipid identifiers to gene symbols responsible for lipid metabolism (64). The log2 z-score standardized values of the corresponding genes were calculated, aimed at finding their lipid correlates. Then, the z-score standardized values of the principal components derived from the glycerolipids (TAGs and DAGs), FFAs, and ACs were correlated with the transcriptomic profiles for the mapped genes using Pearson correlations. We used matching samples from both compartments

to run the correlation analysis. Ingenuity Pathway Analysis based on the top lipid-transcript significant correlations was applied to identify the corresponding enriched pathways. Benjamini-Hochberg procedure was applied to minimize the false discovery rate (FDR) (65).

For differential network analysis aimed at identifying differential lipid correlates (inter- and intra-lipid class) by progression, we obtained the sparse partial correlation networks that capture interdependencies between lipids for the non-progressor and progressor participant groups. We utilized the following approach that leveraged (i) similarity information between lipids that is concordant with data obtained from a diabetic mouse model (Supplement Table 3) and (ii) the assumption that many interconnections, especially across lipid classes, are not present in both groups and hence we can utilize all 92 samples to estimate them more robustly. Throughout the technical developments, p denotes the total number of lipids under consideration, $n_{non-progressor}$ and $n_{progressor}$ denote the sample sizes for non-progressors and progressors, respectively, while x_{ij}^k denotes the relative abundance of lipid j for sample i in condition k (non-progressor, progressor). Further, we arrange the data x_{ij}^k's in matrix form $\mathbf{X}^k$as:

$$\mathbf{X}^k := \begin{bmatrix} x_{11}^k & \cdots & x_{1p}^k \\ \vdots & \ddots & \vdots \\ x_{n_k1}^k & \cdots & x_{n_kp}^k \end{bmatrix}, \quad k \in \{non-progressor, progressor\},$$

and let $\mathbf{X}_j^k$denote its jth column.

The main steps of the proposed estimation procedure include obtaining the lipid grouping structure, the superset of the network skeleton, and the final stabilized network structure. To obtain lipid grouping structure (Step 1), we constructed groups among lipids based on their correlation structure using spectral clustering in progressors and non-progressors (66), and denoted the collections of groups as $\mathcal{G}_{non-progressor}$and $\mathcal{G}_{progressor}$, respectively. In particular,

the number of clusters is pre-specified at 20 for both conditions, hence $\left|\mathcal{G}_{non-progreessor}\right| = \left|\mathcal{G}_{progressor}\right| = 20$. Further, we only retained the groups that were common in both conditions, that is, let $\mathcal{G} = \mathcal{G}_{non-progressor} \cap \mathcal{G}_{progressor}$, and the resulting common group $\mathcal{G}$ contains 7 subsets (groups), primarily encompassing FFAs and selected PCs, TAGs, lysoPCs and lysoPEs, and pPEs. As a confirmatory step, these groups were also detected in the mice serum data (56) where they exhibit strong correlations (co-expression signal). We allowed $\mathcal{G}^c$to denote the indices of lipids that did not belong in any of these 7 groups, that is:

$$\mathcal{G}^c = \{1, \dots, p\} \backslash \{\cup\, g_l, g\_l \in \mathcal{G}\}.$$

To obtain a superset of the network skeleton (Step 2), we estimated the skeleton (edges present) of the non-progressor and progressor partial correlation networks based on a variation of the node-wise regression approach (67), while incorporating lipid group information extracted from Step 1 and encouraging common sparsity structure (absence of edges in both networks) between the two groups (68). Toward this end, by considering the distribution of lipid j conditional on all the other lipids, their relative abundance levels satisfied the following relationship:

$$\mathbf{X}_j^k = \mathbf{X}_{-j}^k \beta_j^k + \mathbf{E}_j, \quad \beta_j^k \in \mathbb{R}^{p-1},$$

where each coordinate of the vector β_j^kencompassed the *scaled partial covariance* of lipid j with all other lipids $j'(j' \neq j)$. Built upon the original node-wise regression formulation (67), to encourage similar sparsity structure incurred by lipids that were within the same group $g \in \mathcal{G}$, we imposed a group-penalty on their coefficients in the form of a vector $\ell_2$norm. On the other hand, for lipids that did not belong to any group, *i.e.*, the elements in $\mathcal{G}^c$, we modeled the coefficient $\beta_{j,j'}^k$ as $\beta_{j,j'}^k = \gamma_{j,j'}^k \theta_{j,j'}, \theta_{j,j'} \geq 01110$ (68) and penalized their individual absolute values to

encourage the presence of common (thus, absence of edges in the networks) across the non-progressor and progressor groups. Formally, the optimization problem was formulated as:

$$\min_{\beta_j^k,\gamma_j^k,\theta_j,j\in\{1,\dots,p\},k\in\{non-progressor,progressor\}} \sum_k \left\{ \sum_{j=1}^{p} \frac{1}{2n_k} \left\| \mathbf{X}_j^k - \mathbf{X}_{-j}^k \beta_j^k \right\|_2^2 + \sum_{g\in\mathcal{G}} \lambda_g \left\| \beta_{j|g}^k \right\|_2 + \eta \sum_{j'\in\mathcal{G}^c} |\gamma_{j,j'}^k| \right\} + \sum_{j\in\mathcal{G}^c} \theta_{j,j'} \quad .(*)$$

The optimization problem in (*) estimated the non-progressor and progressor partial correlation networks *jointly*, thus efficiently utilizing all 106 samples. Further, this objective function is separable in $j = 1, \dots, p$, and thus can be solved by splitting it into p parallel sub-problems. For each sub-problem indexed by j, it is equivalent to solving the following optimization problem obtained after some algebraic manipulations (68) (Lemma 2):

$$\min_{\beta_j^k,k\in\{non-progressor,progressor\}} \sum_k \left\{ \frac{1}{2n_k} \left\| \mathbf{X}_j^k - \mathbf{X}_{-j}^k \beta_j^k \right\|_2^2 + \sum_{g\in\mathcal{G}} \lambda_g \left\| \beta_{j|g}^k \right\|_2 \right\} + \rho \sum_{j\in\mathcal{G}^c} \left(\sum_K |\beta_{j,j'}^k| \right)^{\frac{1}{2}}, where\ \rho = 2\eta^{\frac{1}{2}}. \quad (**)$$

In the above formulation, λ_g, η, ρ were all pre-specified tuning parameters, and they determined the ultimate sparsity level of the estimated networks, through the tuning of the corresponding norms. The solution to (*) contained the skeleton (presence/absence of edges) information of the partial correlation networks of interest; in particular, the nonzero elements in $\widehat{\beta_j^k}$ point to the presence of edges in the network. At this step, we set the tuning parameters at a small relative value, to eliminate edges with a weak signal and to obtain a superset of the network skeleton. We denoted the obtained skeleton superset as $\mathcal{S}^{super}$, and at this step, the estimated skeletons for both conditions corresponded to networks with density level at around 10% (*i.e.* out of the possible $\frac{p^2}{2}$ edges, only 10% are present; for a technical justification of why only sparse partial correlation networks can be estimated from data when the sample size is smaller than the number of lipids (69).

To obtain the final stabilized network structures, we employed the technique of stability selection (70) coupled with the graphical lasso (71) network estimation procedure and also utilized the skeleton information in $\mathcal{S}^{super}$ as follows. We imposed a small lasso penalty for edges that are in $\mathcal{S}^{super}$ and a larger one if in its complement. The stability selection step yielded the final network skeleton structure that was stable and robust to the choice of the tuning parameters, and the networks had a respective density level of 3% (non-progressor) and 2.7% (progressor). Finally, based on the skeleton, we estimated the magnitude of the edges (correlations), which after proper normalization, corresponded to the strength of the partial correlation amongst lipids in the two groups.

Study approval: The study was approved by the Institutional Review Board (IRB)#0000006 at the National Institute of Diabetes, Digestive, and Kidney Diseases, Bethesda, Maryland. All participants gave signed informed consent prior to their participation in the study.

Author contributions: FA designed the lipidomic study, prepared serum samples for mass spectrometry, analyzed and interpreted the data, and wrote the first draft. VN performed the transcriptomic-lipidomic analysis and contributed to manuscript drafting. JL and GM performed the differential network analysis and contributed to manuscript drafting. TMR and JB helped with serum sample preparation for lipidomic analysis and mass spectrometry runs. TS retrieved mass-spectrometry data. HCL and RGN contributed to clinical study design, data collection, manuscript drafting, and critical evaluation of the paper. SP contributed to the lipidomic study design, mass spectrometry, data interpretation and manuscript drafting. All authors have critically evaluated the paper and have approved the final version.

Acknowledgment: Authors would like to thank Lois Jones, RN, Enrique Diaz, RN, Bernadine Waseta, and Camille Waseta for seeing the patients, performing the research studies, and collecting and processing the samples.

Disclosure: KS reports receipt of consult fee from Boerhinger Ingelheim outside the submitted work. TWG reports grants from Zebra Biologics, outside the submitted work. MK reports grants from NIH, non-financial support from the University of Michigan, during the conduct of the study; grants from JDRF, Astra-Zeneca, NovoNordisc, Eli Lilly, Gilead, Goldfinch Bio, Merck, Janssen, and Boehringer-Ingelheim outside the submitted work; also has a patent Biomarkers for CKD progression (encompassing urinary EGF as biomarker of CKD progression) issued. Other authors have declared that no conflict of interest exists.

References:

1. USRDS. Chapter 1: Incidence, Prevalence, Patient Characteristics, and Treatment Modalities https://www.usrds.org/2017/download/v2_c01_IncPrev_17.pdf. 2017.
2. USRDS. United States Renal Data System. 2018 Annual Data Report https://www.usrds.org/2018/view/Default.aspx. 2018.
3. Diabetes 2030 Forecasts, 2015. United States Diabetes Data & Forecasts http://www.altfutures.org/pubs/diabetes2030/UNITEDSTATESDataSheet.pdf. 2015.
4. Rahman M, Yang W, Akkina S, Alper A, Anderson AH, Appel LJ, He J, Raj DS, Schelling J, Strauss L, et al. Relation of serum lipids and lipoproteins with progression of CKD: The CRIC study. *Clin J Am Soc Nephrol.* 2014;9(7):1190-8.
5. Reis A, Rudnitskaya A, Chariyavilaskul P, Dhaun N, Melville V, Goddard J, Webb DJ, Pitt AR, and Spickett CM. Top-down lipidomics of low density lipoprotein reveal altered lipid profiles in advanced chronic kidney disease. *Journal of lipid research.* 2015;56(2):413-22.
6. Reiss AB, Voloshyna I, De Leon J, Miyawaki N, and Mattana J. Cholesterol Metabolism in CKD. *American journal of kidney diseases : the official journal of the National Kidney Foundation.* 2015;66(6):1071-82.
7. Tsuruya K, Yoshida H, Nagata M, Kitazono T, Iseki K, Iseki C, Fujimoto S, Konta T, Moriyama T, Yamagata K, et al. Impact of the Triglycerides to High-Density Lipoprotein Cholesterol Ratio on the Incidence and Progression of CKD: A Longitudinal Study in a Large Japanese Population. *American journal of kidney diseases : the official journal of the National Kidney Foundation.* 2015;66(6):972-83.
8. Wahl P, Ducasa GM, and Fornoni A. Systemic and renal lipids in kidney disease development and progression. *American journal of physiology Renal physiology.* 2016;310(6):F433-45.

9. Quehenberger O, Armando AM, Brown AH, Milne SB, Myers DS, Merrill AH, Bandyopadhyay S, Jones KN, Kelly S, Shaner RL, et al. Lipidomics reveals a remarkable diversity of lipids in human plasma. *Journal of lipid research.* 2010;51(11):3299-305.

10. Quehenberger O, and Dennis EA. The human plasma lipidome. *The New England journal of medicine.* 2011;365(19):1812-23.

11. Graessler J, Schwudke D, Schwarz PE, Herzog R, Shevchenko A, and Bornstein SR. Top-down lipidomics reveals ether lipid deficiency in blood plasma of hypertensive patients. *PLoS One.* 2009;4(7):e6261.

12. Kontush A, Lhomme M, and Chapman MJ. Unraveling the complexities of the HDL lipidome. *Journal of lipid research.* 2013;54(11):2950-63.

13. Pietilainen KH, Sysi-Aho M, Rissanen A, Seppanen-Laakso T, Yki-Jarvinen H, Kaprio J, and Oresic M. Acquired obesity is associated with changes in the serum lipidomic profile independent of genetic effects--a monozygotic twin study. *PLoS One.* 2007;2(2):e218.

14. Stegemann C, Drozdov I, Shalhoub J, Humphries J, Ladroue C, Didangelos A, Baumert M, Allen M, Davies AH, Monaco C, et al. Comparative lipidomics profiling of human atherosclerotic plaques. *Circulation Cardiovascular genetics.* 2011;4(3):232-42.

15. Stegemann C, Pechlaner R, Willeit P, Langley SR, Mangino M, Mayr U, Menni C, Moayyeri A, Santer P, Rungger G, et al. Lipidomics profiling and risk of cardiovascular disease in the prospective population-based Bruneck study. *Circulation.* 2014;129(18):1821-31.

16. Rhee EP, Cheng S, Larson MG, Walford GA, Lewis GD, McCabe E, Yang E, Farrell L, Fox CS, O'Donnell CJ, et al. Lipid profiling identifies a triacylglycerol signature of insulin resistance and improves diabetes prediction in humans. *The Journal of clinical investigation.* 2011;121(4):1402-11.

17. Rhee EP, Clish CB, Ghorbani A, Larson MG, Elmariah S, McCabe E, Yang Q, Cheng S, Pierce K, Deik A, et al. A combined epidemiologic and metabolomic approach improves CKD prediction. *Journal of the American Society of Nephrology : JASN.* 2013;24(8):1330-8.

18. Afshinnia F, Rajendiran TM, Soni T, Byun J, Wernisch S, Sas KM, Hawkins J, Bellovich K, Gipson D, Michailidis G, et al. Impaired beta-Oxidation and Altered Complex Lipid Fatty Acid Partitioning with Advancing CKD. *Journal of the American Society of Nephrology : JASN.* 2018;29(1):295-306.

19. Afshinnia F, Rajendiran TM, Karnovsky A, Soni T, Wang X, Xie D, Yang W, Shafi T, Weir MR, He J, et al. Lipidomic Signature of Progression of Chronic Kidney Disease in the Chronic Renal Insufficiency Cohort. *Kidney Int Rep.* 2016;1(4):256-68.

20. Niewczas MA, Gohda T, Skupien J, Smiles AM, Walker WH, Rosetti F, Cullere X, Eckfeldt JH, Doria A, Mayadas TN, et al. Circulating TNF receptors 1 and 2 predict ESRD in type 2 diabetes. *Journal of the American Society of Nephrology : JASN.* 2012;23(3):507-15.

21. Niewczas MA, Sirich TL, Mathew AV, Skupien J, Mohney RP, Warram JH, Smiles A, Huang X, Walker W, Byun J, et al. Uremic solutes and risk of end-stage renal disease in type 2 diabetes: metabolomic study. *Kidney international.* 2014.

22. Looker HC, Colombo M, Hess S, Brosnan MJ, Farran B, Dalton RN, Wong MC, Turner C, Palmer CN, Nogoceke E, et al. Biomarkers of rapid chronic kidney disease progression in type 2 diabetes. *Kidney international.* 2015;88(4):888-96.

23. Saulnier PJ, Gand E, Velho G, Mohammedi K, Zaoui P, Fraty M, Halimi JM, Roussel R, Ragot S, Hadjadj S, et al. Association of Circulating Biomarkers (Adrenomedullin, TNFR1, and NT-proBNP) With Renal Function Decline in Patients With Type 2 Diabetes: A French Prospective Cohort. *Diabetes care.* 2017;40(3):367-74.

24. Choudhury D, Tuncel M, and Levi M. Diabetic nephropathy -- a multifaceted target of new therapies. *Discovery medicine.* 2010;10(54):406-15.

25. Nowak N, Skupien J, Smiles AM, Yamanouchi M, Niewczas MA, Galecki AT, Duffin KL, Breyer MD, Pullen N, Bonventre JV, et al. Markers of early progressive renal decline in type 2 diabetes suggest different implications for etiological studies and prognostic tests development. *Kidney international.* 2018;93(5):1198-206.

26. Fufaa GD, Weil EJ, Lemley KV, Knowler WC, Brosius FC, 3rd, Yee B, Mauer M, and Nelson RG. Structural Predictors of Loss of Renal Function in American Indians with Type 2 Diabetes. *Clin J Am Soc Nephrol.* 2016;11(2):254-61.

27. Nelson RG, Bennett PH, Beck GJ, Tan M, Knowler WC, Mitch WE, Hirschman GH, and Myers BD. Development and progression of renal disease in Pima Indians with non-insulin-dependent diabetes mellitus. Diabetic Renal Disease Study Group. *The New England journal of medicine.* 1996;335(22):1636-42.

28. Pavkov ME, Knowler WC, Hanson RL, and Nelson RG. Diabetic nephropathy in American Indians, with a special emphasis on the Pima Indians. *Current diabetes reports.* 2008;8(6):486-93.

29. Saulnier PJ, Wheelock KM, Howell S, Weil EJ, Tanamas SK, Knowler WC, Lemley KV, Mauer M, Yee B, Nelson RG, et al. Advanced Glycation End Products Predict Loss of Renal Function and Correlate With Lesions of Diabetic Kidney Disease in American Indians With Type 2 Diabetes. *Diabetes.* 2016;65(12):3744-53.

30. Tanamas SK, Saulnier PJ, Fufaa GD, Wheelock KM, Weil EJ, Hanson RL, Knowler WC, Bennett PH, and Nelson RG. Long-term Effect of Losartan on Kidney Disease in American Indians With Type 2 Diabetes: A Follow-up Analysis of a Randomized Clinical Trial. *Diabetes care.* 2016;39(11):2004-10.

31. Weil EJ, Fufaa G, Jones LI, Lovato T, Lemley KV, Hanson RL, Knowler WC, Bennett PH, Yee B, Myers BD, et al. Effect of losartan on prevention and progression of early diabetic nephropathy in American Indians with type 2 diabetes. *Diabetes.* 2013;62(9):3224-31.

32. Lemley KV, Blouch K, Abdullah I, Boothroyd DB, Bennett PH, Myers BD, and Nelson RG. Glomerular permselectivity at the onset of nephropathy in type 2 diabetes mellitus. *Journal of the American Society of Nephrology : JASN.* 2000;11(11):2095-105.

33. Lemley KV, Boothroyd DB, Blouch KL, Nelson RG, Jones LI, Olshen RA, and Myers BD. Modeling GFR trajectories in diabetic nephropathy. *American journal of physiology Renal physiology.* 2005;289(4):F863-70.

34. Levey AS, Inker LA, Matsushita K, Greene T, Willis K, Lewis E, de Zeeuw D, Cheung AK, and Coresh J. GFR decline as an end point for clinical trials in CKD: a scientific workshop sponsored by the National Kidney Foundation and the US Food and Drug Administration. *American journal of kidney diseases : the official journal of the National Kidney Foundation.* 2014;64(6):821-35.

35. Luo S, Coresh J, Tin A, Rebholz CM, Appel LJ, Chen J, Vasan RS, Anderson AH, Feldman HI, Kimmel PL, et al. Serum Metabolomic Alterations Associated with Proteinuria in CKD. *Clin J Am Soc Nephrol.* 2019;14(3):342-53.

36. Grove KJ, Voziyan PA, Spraggins JM, Wang S, Paueksakon P, Harris RC, Hudson BG, and Caprioli RM. Diabetic nephropathy induces alterations in the glomerular and tubule lipid profiles. *Journal of lipid research.* 2014;55(7):1375-85.

37. Calzada E, Onguka O, and Claypool SM. Phosphatidylethanolamine Metabolism in Health and Disease. *International review of cell and molecular biology.* 2016;321(29-88.

38. Emoto K, Toyama-Sorimachi N, Karasuyama H, Inoue K, and Umeda M. Exposure of phosphatidylethanolamine on the surface of apoptotic cells. *Experimental cell research.* 1997;232(2):430-4.

39. Rockenfeller P, Koska M, Pietrocola F, Minois N, Knittelfelder O, Sica V, Franz J, Carmona-Gutierrez D, Kroemer G, and Madeo F. Phosphatidylethanolamine positively regulates autophagy and longevity. *Cell death and differentiation.* 2015;22(3):499-508.

40. Karaskov E, Scott C, Zhang L, Teodoro T, Ravazzola M, and Volchuk A. Chronic palmitate but not oleate exposure induces endoplasmic reticulum stress, which may contribute to INS-1 pancreatic beta-cell apoptosis. *Endocrinology.* 2006;147(7):3398-407.

41. Sieber J, and Jehle AW. Free Fatty acids and their metabolism affect function and survival of podocytes. *Frontiers in endocrinology.* 2014;5(186.

42. Sieber J, Lindenmeyer MT, Kampe K, Campbell KN, Cohen CD, Hopfer H, Mundel P, and Jehle AW. Regulation of podocyte survival and endoplasmic reticulum stress by fatty acids. *American journal of physiology Renal physiology.* 2010;299(4):F821-9.

43. Soumura M, Kume S, Isshiki K, Takeda N, Araki S, Tanaka Y, Sugimoto T, Chin-Kanasaki M, Nishio Y, Haneda M, et al. Oleate and eicosapentaenoic acid attenuate palmitate-induced inflammation and apoptosis in renal proximal tubular cell. *Biochemical and biophysical research communications.* 2010;402(2):265-71.

44. Martinez-Garcia C, Izquierdo-Lahuerta A, Vivas Y, Velasco I, Yeo TK, Chen S, and Medina-Gomez G. Renal Lipotoxicity-Associated Inflammation and Insulin Resistance Affects Actin Cytoskeleton Organization in Podocytes. *PLoS One.* 2015;10(11):e0142291.

45. Lennon R, Pons D, Sabin MA, Wei C, Shield JP, Coward RJ, Tavare JM, Mathieson PW, Saleem MA, and Welsh GI. Saturated fatty acids induce insulin resistance in human podocytes: implications for diabetic nephropathy. *Nephrology, dialysis, transplantation : official publication of the European Dialysis and Transplant Association - European Renal Association.* 2009;24(11):3288-96.

46. Jiang XS, Chen XM, Wan JM, Gui HB, Ruan XZ, and Du XG. Autophagy Protects against Palmitic Acid-Induced Apoptosis in Podocytes in vitro. *Scientific reports.* 2017;7(42764.

47. Lee E, Choi J, and Lee HS. Palmitate induces mitochondrial superoxide generation and activates AMPK in podocytes. *Journal of cellular physiology.* 2017.

48. Xu S, Nam SM, Kim JH, Das R, Choi SK, Nguyen TT, Quan X, Choi SJ, Chung CH, Lee EY, et al. Palmitate induces ER calcium depletion and apoptosis in mouse podocytes subsequent to mitochondrial oxidative stress. *Cell death & disease.* 2015;6(e1976.

49. Yasuda M, Tanaka Y, Kume S, Morita Y, Chin-Kanasaki M, Araki H, Isshiki K, Araki S, Koya D, Haneda M, et al. Fatty acids are novel nutrient factors to regulate mTORC1 lysosomal localization and apoptosis in podocytes. *Biochimica et biophysica acta.* 2014;1842(7):1097-108.

50. Rhee EP, Souza A, Farrell L, Pollak MR, Lewis GD, Steele DJ, Thadhani R, Clish CB, Greka A, and Gerszten RE. Metabolite profiling identifies markers of uremia. *Journal of the American Society of Nephrology : JASN.* 2010;21(6):1041-51.

51. Otero YF, Stafford JM, and McGuinness OP. Pathway-selective insulin resistance and metabolic disease: the importance of nutrient flux. *The Journal of biological chemistry.* 2014;289(30):20462-9.

52. Song Z, Xiaoli AM, and Yang F. Regulation and Metabolic Significance of De Novo Lipogenesis in Adipose Tissues. *Nutrients.* 2018;10(10).

53. Carlson CA, and Kim KH. Regulation of hepatic acetyl coenzyme A carboxylase by phosphorylation and dephosphorylation. *Archives of biochemistry and biophysics.* 1974;164(2):478-89.

54. Gillies CE, Putler R, Menon R, Otto E, Yasutake K, Nair V, Hoover P, Lieb D, Li S, Eddy S, et al. An eQTL Landscape of Kidney Tissue in Human Nephrotic Syndrome. *Am J Hum Genet.* 2018;103(2):232-44.

55. Sieber J, Weins A, Kampe K, Gruber S, Lindenmeyer MT, Cohen CD, Orellana JM, Mundel P, and Jehle AW. Susceptibility of podocytes to palmitic acid is regulated by stearoyl-CoA desaturases 1 and 2. *The American journal of pathology.* 2013;183(3):735-44.

56. Sas KM, Lin J, Rajendiran TM, Soni T, Nair V, Hinder LM, Jagadish HV, Gardner TW, Abcouwer SF, Brosius FC, 3rd, et al. Shared and distinct lipid-lipid interactions in plasma and affected tissues in a diabetic mouse model. *Journal of lipid research.* 2018;59(2):173-83.

57. Li Y, Chung S, Li Z, Overstreet JM, Gagnon L, Grouix B, Leduc M, Laurin P, Zhang MZ, and Harris RC. Fatty acid receptor modulator PBI-4050 inhibits kidney fibrosis and improves glycemic control. *JCI Insight.* 2018;3(10).

58. Afshinnia F, Rajendiran TM, Wernisch S, Soni T, Jadoon A, Karnovsky A, Michailidis G, and Pennathur S. Lipidomics and Biomarker Discovery in Kidney Disease. *Seminars in nephrology.* 2018;38(2):127-41.

59. Sas KM, Kayampilly P, Byun J, Nair V, Hinder LM, Hur J, Zhang H, Lin C, Qi NR, Michailidis G, et al. Tissue-specific metabolic reprogramming drives nutrient flux in diabetic complications. *JCI Insight.* 2016;1(15):e86976.

60. Cohen CD, Frach K, Schlondorff D, and Kretzler M. Quantitative gene expression analysis in renal biopsies: a novel protocol for a high-throughput multicenter application. *Kidney international.* 2002;61(1):133-40.

61. Schmid H, Boucherot A, Yasuda Y, Henger A, Brunner B, Eichinger F, Nitsche A, Kiss E, Bleich M, Grone HJ, et al. Modular activation of nuclear factor-kappaB transcriptional programs in human diabetic nephropathy. *Diabetes.* 2006;55(11):2993-3003.

62. Overmyer KA, Evans CR, Qi NR, Minogue CE, Carson JJ, Chermside-Scabbo CJ, Koch LG, Britton SL, Pagliarini DJ, Coon JJ, et al. Maximal oxidative capacity during exercise is associated with skeletal muscle fuel selection and dynamic changes in mitochondrial protein acetylation. *Cell metabolism.* 2015;21(3):468-78.

63. Muller CJ, and MacLehose RF. Estimating predicted probabilities from logistic regression: different methods correspond to different target populations. *International journal of epidemiology.* 2014;43(3):962-70.

64. Karnovsky A, Weymouth T, Hull T, Tarcea VG, Scardoni G, Laudanna C, Sartor MA, Stringer KA, Jagadish HV, Burant C, et al. Metscape 2 bioinformatics tool for the analysis and visualization of metabolomics and gene expression data. *Bioinformatics.* 2012;28(3):373-80.

65. Benjamini Y, and Hochberg Y. Controlling the false discovery rate: a practical and powerful approach to multiple testing. *Journal of the Royal Statistical Society, Series B.* 1995;57(1):289-300.

66. Ng AY, Jordan MI, and Weiss Y. *Advances in Neural Information Processing Systems* 2002:849-56.

67. Meinshausen N, and Buhlmann P. High-dimensional graphs and variable selection with the lasso. *The Annals of Statistics.* 2006;34(3):1436-62.

68. Guo J, Levina E, Michailidis G, and Zhu J. Joint estimation of multiple graphical models. *Biometrika.* 2011;98(1):1-15.

69. Basu S, Duren W, Evans CR, Burant CF, Michailidis G, and Karnovsky A. Sparse network modeling and metscape-based visualization methods for the analysis of large-scale metabolomics data. *Bioinformatics.* 2017;33(10):1545-53.

70. Meinshausen N, and Bühlmann P. Stability selection. *Journal of the Royal Statistical Society: Series B (Statistical Methodology).* 2010;72(4):417-73.

71. Friedman J, Hastie T, and Tibshirani R. Sparse inverse covariance estimation with the graphical lasso. *Biostatistics.* 2008;9(3):432-41.

Figure Legends:

Figure 1: Flow diagram of analytical strategy and post-trial follow up of participants of the "Renoprotection in Early Diabetic Nephropathy in Pima Indians" trial analyzed in this study.

Figure 2: Baseline and last measured GFR in 32 progressors and 60 non-progressors. The boxes represent median and interquartile range and bars represent 1.5-fold×the interquartile range below the 25th percentile and above the 75th percentile. Outliers outside the mean + 2 SD are shown with dots. GFR, glomerular filtration rate.

Figure 3: Differences in carbon chain length and number of double bonds in complex lipids and acylcarnitines between progressors and non-progressors (total N=92 in all panels). Abundance of TAGs and ACs were measured at the baseline visit of this study and compared in progressors and non-progressors. **A.** In serum from progressors (N=32), there was a greater relative abundance of longer TAGs with more double bonds. An opposite trend was observed in non-progressors (N=60). **B.** A similar pattern was found when all participants (progressors + non-progressors) were grouped based on whether or not they achieved a sustained GFR<90 (N=33), <60 (N=13), and <30 mL/min (N=6). Bonferroni threshold for multiple comparisons was set to 0.0063 (0.05 divided by 8 panels per class). **C.** In progressors (N=32), there was a lower relative abundance of longer ACs with more double bonds. An opposite trend was observed in non-progressors (N=60). **D.** A similar trend was noted in abundance of ACs by carbon number, when all participants were grouped based on whether or not they achieved a sustained GFR<90 (N=33), <60 (N=13), or <30 mL/min (N=6). Bonferroni threshold for multiple comparisons was set to 0.0063 (0.05 divided by 8 panels per class). P values are products of testing abundance of lipid by "carbon number × double bond" interaction term in

progressors versus non-progressors using mixed-linear models. GFR, glomerular filtration rate; AC, acylcarnitine; TAG, triacylglycerol.

Figure 4: Adjusted correlation of long (C16-20) to intermediate chain (C6-14) acylcarnitine ratio with complex lipid of various chain length and double bonds. Long-to-intermediate AC ratio is directly correlated with shorter complex lipids with fewer double bonds, but is inversely correlated with longer complex lipids with more double bonds in CE class. P values are product of testing partial correlation coefficients in multiple linear regression models adjusting for sex and ACR. AC, acylcarnitine; CE, cholesteryl ester; DAG, diacylglycerol; PE, phosphatidylethanolamine; pPE, plasmenyl-PE; TAG, triacylglycerol.

Figure 5: AC alterations by categories of baseline ACR in progressors and non-progressors. ACs of various chain length and double bonds were quantified in serum at the baseline visit of progressors and non-progressors. Distribution of various ACs by ACR category revealed lower levels of C16-C20 ACs from non-progressors with normoalbuminuria (upper left) to progressors with ACR>300 mg/g (lower right). Within each ACR category, long chain AC abundance (C16-20) increased in non-progressors with ACR 30-299 mg/g ($p=0.006$) and decreased in progressors with ACR>300 mg/g ($p<0.0001$). Sample size 43 in ACR<30, 33 in ACR 30-299, and 16 in ACR≥300 mg/g. Bonferroni threshold for multiple comparisons was set to 0.0083 (0.05 divided by 6 panels). P values are products of testing abundance of lipid by "carbon number × double bond" interaction term in progressors versus non-progressors using mixed-linear models. ACR, albumin-creatinine ratio; AC, acylcarnitines.

Figure 6: Predicting DKD progression with probabilistic risk scores. Probabilistic risk score derived from odds of progression by three different models were compared. Model 1 incorporated baseline ACR and GFR (ACR+GFR), Model 2 incorporated independent lipid factors predicting

progression (Lipids), and Model 3 consisted of the lipids plus baseline ACR and GFR (ACR+GFR+Lipids). Progressors (N=32) had a higher probabilistic risk scores compared with non-progressors (N=60) in all models, and the largest score was noted in Model 3, when lipids were included with baseline ACR and GFR. Bar graphs are mean and error bars are 1 SD above and below the mean.

Figure 7: Differential network Analysis. To identify inter- and intra-class lipid correlates, we obtained the sparse partial correlation networks that captured the interdependencies between lipids. We utilized lipid grouping structure, obtained the superset of the network skeleton, and finally obtained the final stable network structures, the latter based on a bootstrapping method. Differential network analysis revealed differential loss of edges between various lipid classes in progressors characterized by 547 significant edges versus 1028 in non-progressors ($p<0.0001$) out of 55,460 possible permutations of bivariate correlations. The lines represent significant edges that were exclusively observed in non-progressors (blue) or progressors (red). Common edges are shown in gray. The node size is proportional to the number of connectivity levels within and across lipid subclasses, and node colors represent number of cross-class connections (white=low, yellow=middle, red=high). Nodes are categorized by chain length (bottom, middle, top), and double bonds (low, high) with details shown in Supplement Table 3.

Figure 8: Integrative transcriptomic-lipidomic analysis identifies G-protein coupled signaling pathways and nuclear hormone-activating receptors in regulation of fatty acid synthesis and β-oxidation. Ingenuity Pathway Analysis reveals enrichment of G-Protein signaling pathways involved in regulation of NF-kB, CREB, and STAT3 in glomerular **(A)** and tubulointerstitial compartments **(B)**. CREB is transcriptional regulator of *de novo* lipogenesis. Genes regulating the intermediaries highlighted in purple in panels A and B are significantly

correlated with the corresponding serum lipids. The genes downstream of nuclear hormone-activating receptor PPARG known to regulate fatty acid metabolism and their β-oxidation in both glomerular **(C)** and tubulointerstitial compartments **(D)** are significantly correlated with serum lipids identified via the lipidomic analysis. NF-kB, nuclear Factor kappa-light-chain-enhancer of activated B cells); CREB, cAMP response element-binding protein; NF-kB, nuclear Factor kappa-light-chain-enhancer of activated B cells; PPARG, peroxisome proliferator-activated receptor gamma; STAT3, signal transducer and activator of transcription 3**.**

Figure 9: Proposed mechanisms underlying lipid abnormalities that predict early renal function decline in DKD. Upregulation of ACC, mediated by insulin resistance, enhances *de novo* lipogenesis characterized by increased abundance of palmitate, a C16 fatty acid. With elongation and desaturation, palmitate is converted into longer unsaturated fatty acids, which are incorporated into complex lipids (*e.g.,* glycerolipids). In concert, upregulation of ACC also inhibits CPT1, which in turn decreases the conversion of L-carnitine to C16-20 acylcarnitines. C16-20 acylcarnitines are efficient β-oxidation substrates and, therefore, their diminished mitochondrial transfer downregulates β-oxidation. The net effect of upregulated *de novo* lipogenesis is characterized by higher abundance of longer chain polyunsaturated glycerolipids and lower abundance of C16-20 acylcarnitines and shorter low-double-bond glycerolipids. *ACACA*, acetyl Co-A carboxylase alpha; *ACLY*, ATP citrate lyase; *ACS*, acetyl Co-A synthetase; *CPT*, carnitine palmitoyltransferase; *DEGS*, delta 4-desaturase; *ELOVL*, elongation of very long chain fatty acids; *FASN*, fatty acid synthase; *FADS*, fatty acid desaturase; *SCD*, stearoyl-Coenzyme A desaturase; PE, phosphatidylethanolamine; FFA, free fatty acid; SLDB TAG, short low double bond triacylglycerol.

Table 1: Comparing baseline characteristics and follow up of progressors and non-progressors.

	Non-progressors N=60	**Progressors N=32**	**p value**
Duration of follow ups, years	8.8 ± 3.0	8.9 ± 3.0	0.932
Number of follow up visits	10 ± 4	10 ± 3	0.827
Age, years	46 ± 9	43 ± 9	0.120
Male sex, n (%)	20 (33.3)	5 (15.6)	0.069
Body mass index, kg/m^2	36.2 ± 8.3	34.5 ± 8.0	0.355
Systolic blood pressure, mmHg	122 ± 15	127 ± 18	0.193
Diastolic blood pressure, mmHg	76 ± 9	81 ± 9	0.010
Fasting plasma glucose, mg/dL	207.2 ± 90.5	262.3 ± 108.7	0.011
HbA1c, %	9.0 ± 2.3	10.2 ± 1.9	0.012
Total cholesterol, mg/dL	167.0 ± 35.6	184.9 ± 47.4	0.071
Triglyceride, mg/dL	180.4 ± 136.6	273.6 ± 283.3	0.137
Total serum protein, g/dL	6.8 ± 0.4	6.8 ± 0.5	0.851
Serum Albumin, g/dL	3.5 ± 0.4	3.4 ± 0.4	0.166
AST, IU/L	24.9 ± 20.3	23.6 ± 22.4	0.802
Serum alkaline phosphatase, IU/L	107.5 ± 32.8	118.6 ± 35.3	0.160
Total bilirubin, mg/dL	0.5 ± 0.2	0.4 ± 0.2	0.067
GFR, mL/min	149 ± 46	170 ± 51	0.038
Urine ACR, median [IQR], mg/g	19 [9 – 66]	77 [50 – 396]	<0.001
Intervention arm, n (%)	36 (60.0)	15 (46.9)	0.228
Medications:			
Antihypertensive, n (%)	24 (40.0)	13 (40.6)	0.954
Insulin, n (%)	23 (38.3)	16 (50.0)	0.281
Oral hypoglycemic, n (%)	48 (80.0)	25 (78.1)	0.832
Statins, n (%)	10 (16.7)	9 (28.1)	0.196
Other lipid lowering, n (%)	12 (20.0)	10 (31.3)	0.228

[a] Means with standard deviations are given for continuous variables.

ACR, albumin-creatinine ratio; AST, aspartate aminotransferase; GFR, glomerular filtration rate; HbA1c, hemoglobin A1c; IQR, interquartile range.

Table 2: Hazard ratios of lipid predictors of DKD progression (40% decline in GFR).

Predictors	Hazard rate ratio	95% CI	p value	FDR
Model 1 (Base model)				
Unsaturated PE (1SD)	1.78	1.24 to 2.57	0.002	0.025
Unsaturated FFA (1SD)	0.66	0.46 to 0.95	0.026	0.050
Model 2 (Model 1 + AC, TAG interaction with ACR)				
Unsaturated PE (1SD)	2.36	1.56 to 3.58	<0.001	0.01
Unsaturated FFA (1SD)	0.59	0.41 to 0.84	0.004	0.03
C16-20 AC (1SD change in ACR<30)	3.36	1.00 to 11.28	0.05	0.05
C16-20 AC (1SD change in ACR30-299)	2.39	0.84 to 6.49	0.103	0.06
SLDB TAG (1SD change in ACR<30)	0.25	0.09 to 0.66	0.005	0.04
SLDB TAG (1SD change in ACR30-299)	0.19	0.07 to 0.52	0.001	0.02
Model 3 (Model 2 + GFR + ACR)				
Unsaturated PE (1SD)	2.57	1.66 to 3.98	<0.001	0.008
Unsaturated FFA (1SD)	0.54	0.36 to 0.79	0.002	0.023
C16-20 AC (1SD change in ACR<30)	4.07	1.03 to 16.06	0.045	0.053
C16-20 AC (1SD change in ACR30-299)	2.44	0.78 to 7.62	0.125	0.060
SLDB TAG (1SD change in ACR<30)	0.16	0.05 to 0.52	0.002	0.025
SLDB TAG (1SD change in ACR30-299)	0.14	0.05 to 0.41	<0.001	0.015
GFR (mL/min)	1.009	1.002 to 1.017	0.015	0.045
ACR (mg/g)	1.001	1.000 to 1.001	0.006	0.038

[a] Model 1 or base model shows independent lipids without adjustment with baseline ACR and GFR. [b] Model 2 is model 1 plus an interaction term of C16-20 AC and short, low-double-bond TAGs by ACR category with ACR>300 being the reference category. [c] Model 3 is model 2 plus baseline GFR and ACR independent of HbA1c and fasting plasma glucose.

AC, acylcarnitine; ACR, albumin creatinine ratio; CI, confidence interval; FDR, false discovery rate; FFA, free fatty acid; GFR, iothalamate-based glomerular filtration rate; PE, phosphatidylethanolamine; SLDB TAG, short, low-double-bond triacylglycerol.

Table 3: Proportion of progressors by quartiles of the probabilistic risk scores calculated by various models

	Quartile 1 N=23	Quartile 2 N=23	Quartile 3 N=23	Quartile 4 N=23	p value (trend)
Model 1 (ACR+GFR)	13.04 (7.18)	21.74 (8.794)	52.17 (10.65)	52.17 (10.65)	0.001
Model 2 (Lipids)	17.39 (8.081)	17.39 (8.081)	43.48 (10.569)	60.87 (10.405)	0.0005
Model 3 (ACR+GFR+Lipids)	4.35 (4.348)	8.7 (6.007)	47.83 (10.65)	78.26 (8.794)	<0.0001

Note: The third and fourth quartiles of the risk score Model 1 (ACR+GFR) and the first and the second quartiles of Model 2 (Lipids) were not discriminatory. However, the most discrimination was obtained in Model 3 when lipids were combined with baseline ACR and GFR. Values are percentage of progressors and standard error. N in each quartile is 23. ACR, albumin-creatinine ratio; GFR, glomerular filtration rate

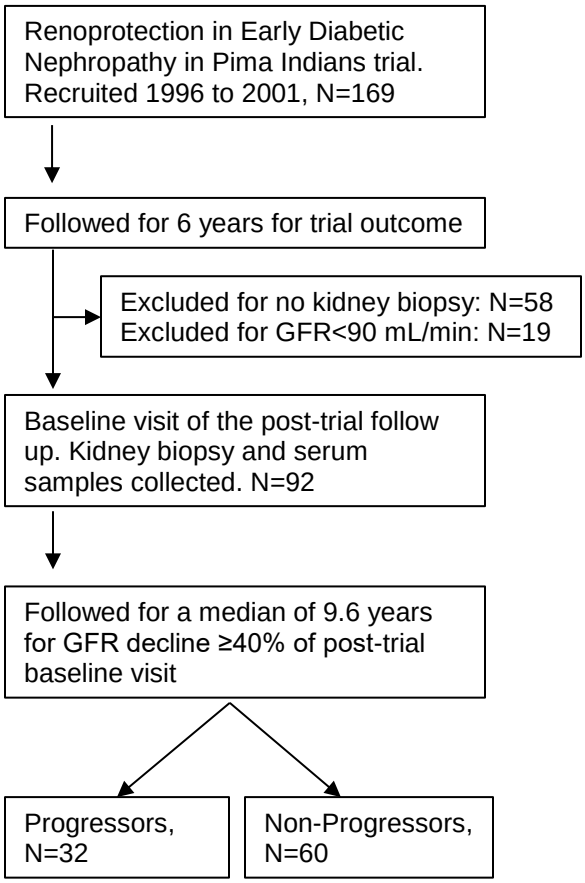

Figure 1: Flow diagram of analytical strategy and post-trial follow up of participants of the "Renoprotection in Early Diabetic Nephropathy in Pima Indians" trial analyzed in this study.

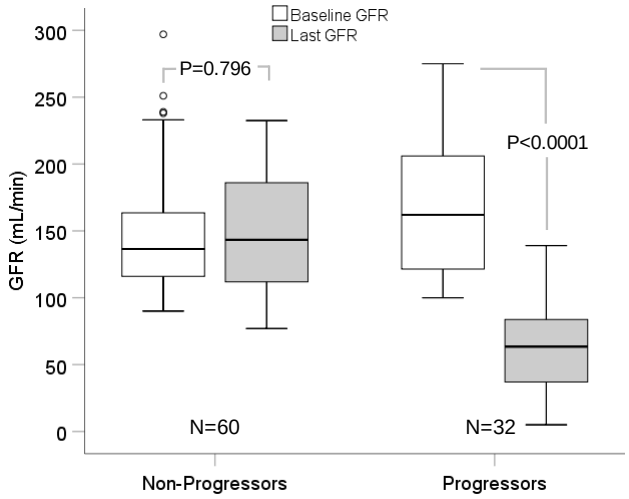

Figure 2: Baseline and last measured GFR in 32 progressors and 60 non-progressors. The boxes represent median and interquartile range and bars represent 1.5-fold×the interquartile range below the 25th percentile and above the 75th percentile. Outliers outside the mean + 2 SD are shown with dots. GFR, glomerular filtration rate.

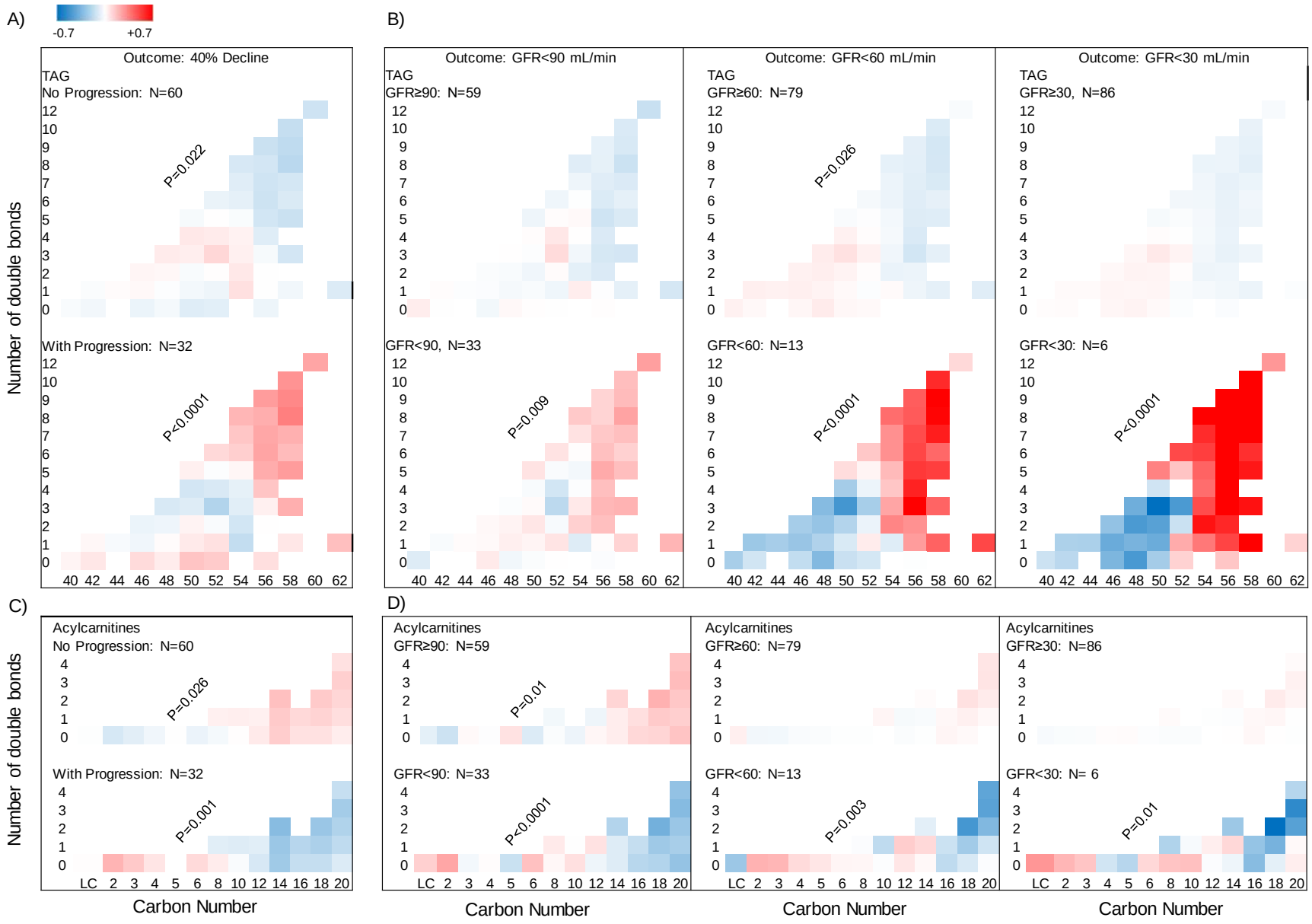
A)
-0.7
+0.7
B)
Outcome: 40% Decline
Outcome: GFR<90 mL/min
Outcome: GFR<60 mL/min
Outcome: GFR<30 mL/min
TAG
No Progression: N=60
With Progression: N=32
GFR≥90: N=59
GFR<90, N=33
GFR≥60: N=79
GFR<60: N=13
GFR≥30, N=86
GFR<30: N=6
P=0.022
P<0.0001
P=0.009
P=0.026
P<0.0001
P<0.0001
Number of double bonds
C)
D)
Acylcarnitines
No Progression: N=60
With Progression: N=32
GFR≥90: N=59
GFR<90: N=33
GFR≥60: N=79
GFR<60: N=13
GFR≥30: N=86
GFR<30: N= 6
P=0.026
P=0.001
P=0.01
P<0.0001
P=0.003
P=0.01
LC 2 3 4 5 6 8 10 12 14 16 18 20
40 42 44 46 48 50 52 54 56 58 60 62
Carbon Number

Figure 3: Differences in carbon chain length and number of double bonds in complex lipids and acylcarnitines between progressors and non-progressors (total N=92 in all panels). Abundance of TAGs and ACs were measured at the baseline visit of this study and compared in progressors and non-progressors. **A.** In serum from progressors (N=32), there was a greater relative abundance of longer TAGs with more double bonds. An opposite trend was observed in non-progressors (N=60). **B.** A similar pattern was found when all participants (progressors + non-progressors) were grouped based on whether or not they achieved a sustained GFR<90 (N=33), <60 (N=13), and <30 mL/min (N=6). Bonferroni threshold for multiple comparisons was set to 0.0063 (0.05 divided by 8 panels per class). **C.** In progressors (N=32), there was a lower relative abundance of longer ACs with more double bonds. An opposite trend was observed in non-progressors (N=60). **D.** A similar trend was noted in abundance of ACs by carbon number, when all participants were grouped based on whether or not they achieved a sustained GFR<90 (N=33), <60 (N=13), or <30 mL/min (N=6). Bonferroni threshold for multiple comparisons was set to 0.0063 (0.05 divided by 8 panels per class). P values are products of testing abundance of lipid by "carbon number × double bond" interaction term in progressors versus non-progressors using mixed-linear models. GFR, glomerular filtration rate; AC, acylcarnitine; TAG, triacylglycerol.

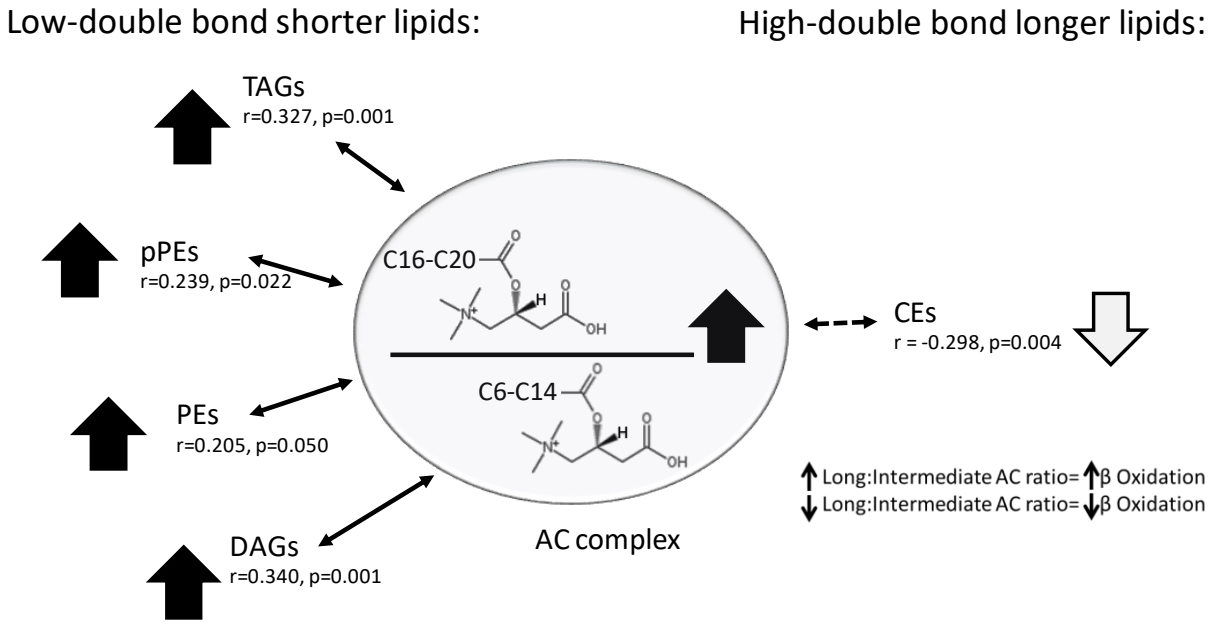

Figure 4: Adjusted correlation of long (C16-20) to intermediate chain (C6-14) acylcarnitine ratio with complex lipid of various chain length and double bonds. Long-to-intermediate AC ratio is directly correlated with shorter complex lipids with fewer double bonds, but is inversely correlated with longer complex lipids with more double bonds in CE class. P values are product of testing partial correlation coefficients in multiple linear regression models adjusting for sex and ACR. AC, acylcarnitine; CE, cholesteryl ester; DAG, diacylglycerol; PE, phosphatidylethanolamine; pPE, plasmenyl-PE; TAG, triacylglycerol.

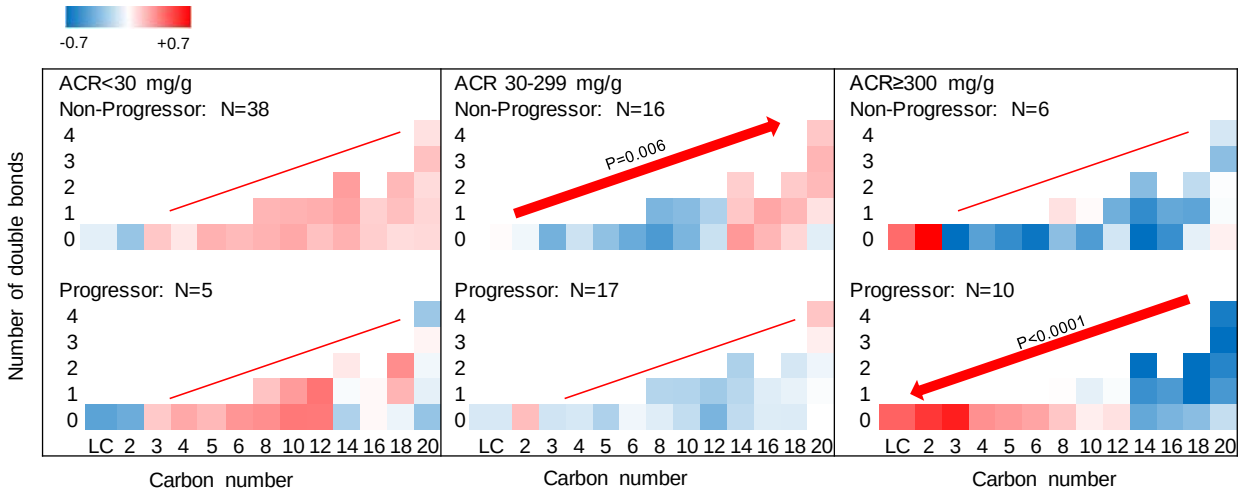

Figure 5: AC alterations by categories of baseline ACR in progressors and non-progressors. ACs of various chain length and double bonds were quantified in serum at the baseline visit of progressors and non-progressors. Distribution of various ACs by ACR category revealed lower levels of C16-C20 ACs from non-progressors with normoalbuminuria (upper left) to progressors with ACR>300 mg/g (lower right). Within each ACR category, long chain AC abundance (C16-20) increased in non-progressors with ACR 30-299 mg/g (p=0.006) and decreased in progressors with ACR>300 mg/g (p<0.0001). Sample size 43 in ACR<30, 33 in ACR 30-299, and 16 in ACR≥300 mg/g. Bonferroni threshold for multiple comparisons was set to 0.0083 (0.05 divided by 6 panels). P values are products of testing abundance of lipid by "carbon number × double bond" interaction term in progressors versus non-progressors using mixed-linear models. ACR, albumin-creatinine ratio; AC, acylcarnitines.

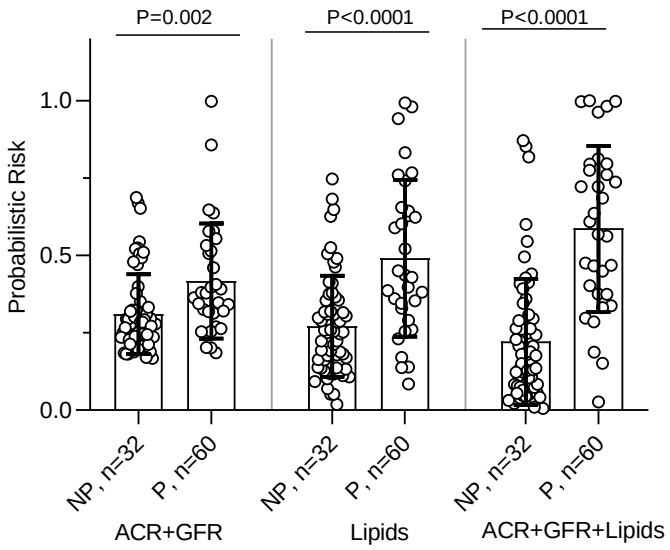

Figure 6: Predicting DKD progression with probabilistic risk scores. Probabilistic risk score derived from odds of progression by three different models were compared. Model 1 incorporated baseline ACR and GFR (ACR+GFR), Model 2 incorporated independent lipid factors predicting progression (Lipids), and Model 3 consisted of the lipids plus baseline ACR and GFR (ACR+GFR+Lipids). Progressors (N=32) had a higher probabilistic risk scores compared with non-progressors (N=60) in all models, and the largest score was noted in Model 3, when lipids were included with baseline ACR and GFR. Bar graphs are mean and error bars are 1 SD above and below the mean.

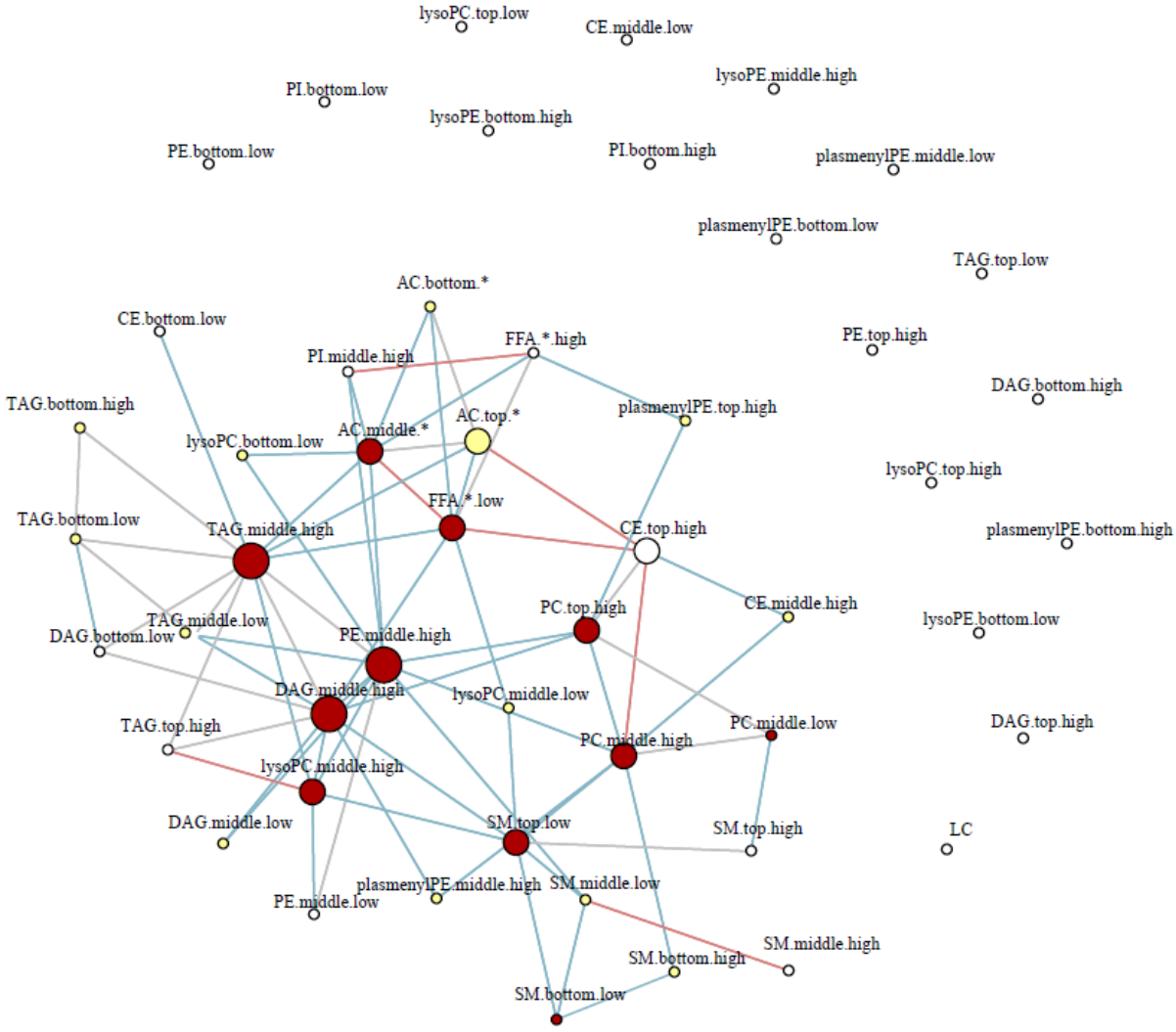

Figure 7: Differential network Analysis. To identify inter- and intra-class lipid correlates, we obtained the sparse partial correlation networks that captured the interdependencies between lipids. We utilized lipid grouping structure, obtained the superset of the network skeleton, and finally obtained the final stable network structures, the latter based on a bootstrapping method. Differential network analysis revealed differential loss of edges between various lipid classes in progressors characterized by 547 significant edges versus 1028 in non-progressors ($p<0.0001$) out of 55,460 possible permutations of bivariate correlations. The lines represent significant edges that were exclusively observed in non-progressors (blue) or progressors (red). Common edges are shown in gray. The node size is proportional to the number of connectivity levels within and across lipid subclasses, and node colors represent number of cross-class connections (white=low, yellow=middle, red=high). Nodes are categorized by chain length (bottom, middle, top), and double bonds (low, high) with details shown in Supplement Table 3.

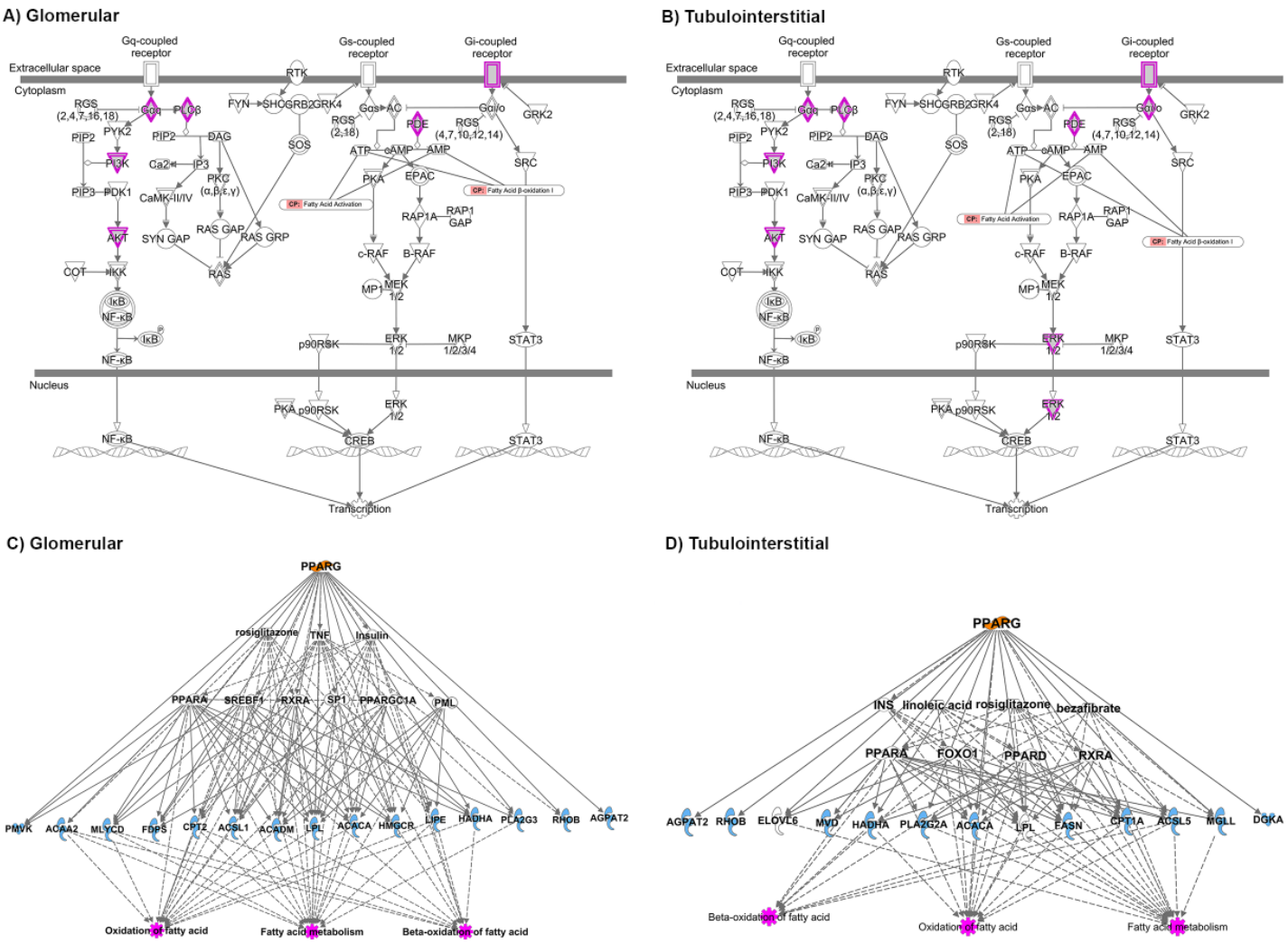

Figure 8: Integrative transcriptomic-lipidomic analysis identifies G-protein coupled signaling pathways and nuclear hormone-activating receptors in regulation of fatty acid synthesis and β-oxidation. Ingenuity Pathway Analysis reveals enrichment of G-Protein signaling pathways involved in regulation of NF-kB, CREB, and STAT3 in glomerular **(A)** and tubulointerstitial compartments **(B)**. CREB is transcriptional regulator of *de novo* lipogenesis. Genes regulating the intermediaries highlighted in purple in panels A and B are significantly correlated with the corresponding serum lipids. The genes downstream of nuclear hormone-activating receptor PPARG known to regulate fatty acid metabolism and their β-oxidation in both glomerular **(C)** and tubulointerstitial compartments **(D)** are significantly correlated with serum lipids identified via the lipidomic analysis. NF-kB, nuclear Factor kappa-light-chain-enhancer of activated B cells); CREB, cAMP response element-binding protein; NF-kB, nuclear Factor kappa-light-chain-enhancer of activated B cells; PPARG, peroxisome proliferator-activated receptor gamma; STAT3, signal transducer and activator of transcription 3**.**

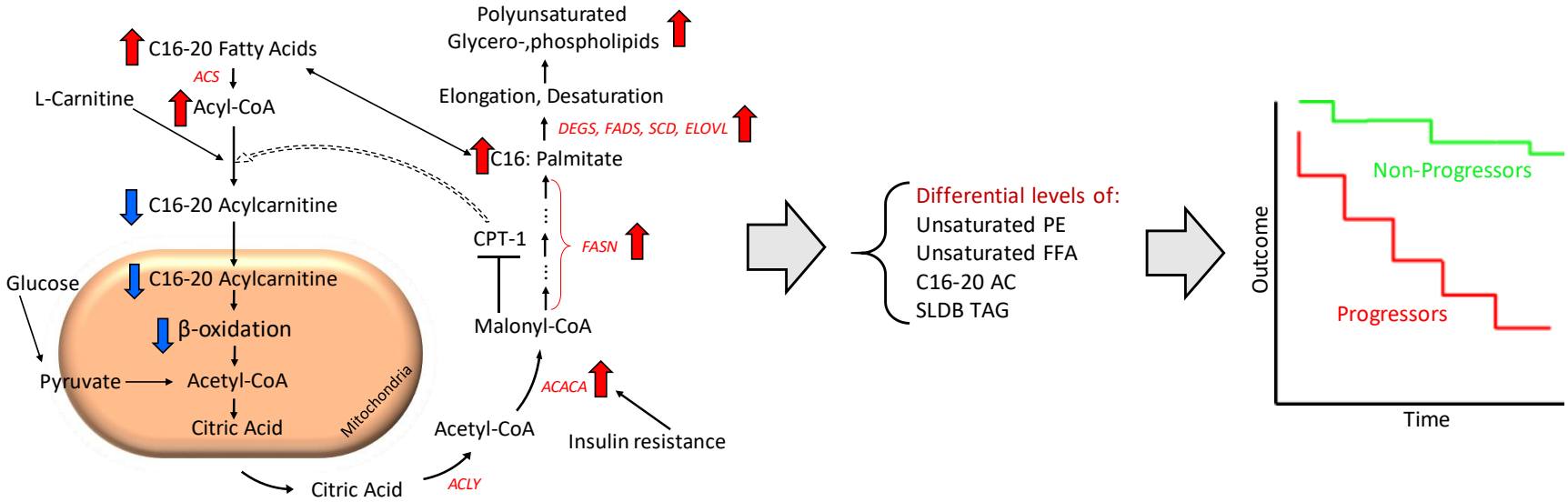

Figure 9: Proposed mechanisms underlying lipid abnormalities that predict early renal function decline in DKD. Upregulation of ACC, mediated by insulin resistance, enhances *de novo* lipogenesis characterized by increased abundance of palmitate, a C16 fatty acid. With elongation and desaturation, palmitate is converted into longer unsaturated fatty acids, which are incorporated into complex lipids (*e.g.*, glycerolipids). In concert, upregulation of ACC also inhibits CPT1, which in turn decreases the conversion of L-carnitine to C16-20 acylcarnitines. C16-20 acylcarnitines are efficient β-oxidation substrates and, therefore, their diminished mitochondrial transfer downregulates β-oxidation. The net effect of upregulated *de novo* lipogenesis is characterized by higher abundance of longer chain polyunsaturated glycerolipids and lower abundance of C16-20 acylcarnitines and shorter low-double-bond glycerolipids. *ACACA*, acetyl Co-A carboxylase alpha; *ACLY*, ATP citrate lyase; *ACS*, acetyl Co-A synthetase; *CPT*, carnitine palmitoyltransferase; *DEGS*, delta 4-desaturase; *ELOVL*, elongation of very long chain fatty acids; *FASN*, fatty acid synthase; *FADS*, fatty acid desaturase; *SCD*, stearoyl-Coenzyme A desaturase; PE, phosphatidylethanolamine; FFA, free fatty acid; SLDB TAG, short low double bond triacylglycerol.